

Constraining Mineralogical Composition of Asteroid Ryugu with Ground-Based Observations

Lucille Le Corre¹, Vishnu Reddy², Juan A. Sanchez¹, Driss Takir³, Ed A. Cloutis⁴, Audrey Thirouin⁵, Jian-Yang Li¹, Seiji Sugita⁶, Eri Tatsumi⁶.

¹*Planetary Science Institute, Tucson, Arizona, USA*

²*Lunar and Planetary Laboratory, University of Arizona, Tucson, Arizona, USA*

³*SETI Institute, Mountain View, CA, USA*

⁴*Department of Geography, University of Winnipeg, Winnipeg, Manitoba, Canada*

⁵*Lowell Observatory, Flagstaff, AZ, USA*

⁶*Dept. of Earth and Planetary Science, University of Tokyo, Tokyo, Japan*

In preparation for the arrival of the Japanese Space Agency's (JAXA) Hayabusa2 sample return mission to near-Earth asteroid (NEA) (162173) Ryugu, we took the opportunity to characterize the target with a ground-based telescope. We observed Ryugu using the SpeX instrument in Prism mode on NASA Infrared Telescope Facility (IRTF) on Mauna Kea, Hawaii, on July, 12 2016 when the asteroid was 18.87 visual magnitude, at a phase angle of 13.3°. The NIR spectra were used to constrain Ryugu's surface composition, determine meteorite analogs and study spectral affinity to other asteroids. We also modeled its photometric properties using archival data. Using the Lommel-Seeliger model we computed the predicted flux for Ryugu at a wide range of viewing geometries as well as albedo quantities such as geometric albedo, phase integral, and spherical Bond albedo. Our computed albedo quantities are consistent with results from Ishiguro et al. (2014). In previous work, Ryugu's visible spectrum revealed that it can be classified as a C-type object. In addition, not all previous ground-based observations of Ryugu detected the 0.7 μm absorption feature due to the presence of phyllosilicates. Our spectrum of Ryugu has a broad absorption band at 1 μm , a slope change at 1.6 μm , and a second broad absorption band near 2.2 μm , but no well-defined absorption features over the 0.8-2.5 μm range. The two broad absorption features, if confirmed, are consistent with CO and CV chondrites. We computed the Reflectance Factor (REFF) of Ryugu at 550 nm, which is consistent with the reflectance measured for the CM and CI carbonaceous chondrite groups. Samples of CO and CV chondrites are usually brighter and less red sloped than Ryugu. It is interesting to note that recent work suggested space weathering could darken and redden the spectra of carbonaceous chondrites. Our spectrum of Ryugu is different from previously published spectra showing a more neutral spectral slope, however, this is not the only object with this kind of spectral shape. The shape matches very well those of NEA (85275) 1994 LY and Mars-crossing asteroid (316720) 1998 BE7, suggesting that their surface regolith have similar composition. With a semi-major axis of ~ 1.9 AU, and NEA 1994 LY may come from the inner part of the main asteroid belt. Asteroid 1998 BE7, with a semi-major axis of ~ 3 AU, probably formed far in the outer part of the main belt. The differences observed between the spectra of these asteroids could be explained by differences in composition, grain size, space weathering, and phase angle. We also compared the spectrum of Ryugu with that of main belt asteroid (302) Clarissa, the largest asteroid in the Clarissa asteroid family, suggested as a possible source of Ryugu by Campins et al. (2013). We found that the spectrum of Clarissa shows significant differences with our NIR spectrum of Ryugu. Our analysis shows Ryugu's spectrum best matches two CM2 carbonaceous chondrites, Mighei and ALH83100. Previous work suggested CM and CI carbonaceous chondrites are the most consistent with Ryugu's spectra. We expect the surface regolith of Ryugu to be altered by a range of factors including temperature, contamination by exogenic material, and space weathering, posing challenges to link spacecraft and ground-based data, and sample site selection.

References

[1] Campins et al. (2013), *The Astronomical Journal*, 146:26. [2] Ishiguro et al. (2014), *The Astrophysical Journal*, 792, 74.

3- μm SPECTROSCOPY OF WATER-RICH METEORITES AND ASTEROIDS: NEW RESULTS AND IMPLICATIONS

D. Takir¹, J. P. Emery², C.A., Hibbitts³, ¹SETI Institute, Mountain View, CA 94043, USA; ²University of Tennessee, Knoxville, TN 37996, USA; ³JHU Applied Physics Laboratory, Laurel, MD 20723-6005, USA.

Introduction: Ground-based observations of water-rich asteroids are important to constrain many questions related to the abundance and distribution of volatiles in the early Solar System, and to the evolution of many diverse Solar System bodies. Recent studies have revealed that several airless bodies, including the Moon and asteroid Psyche ([1], [2], [3], [4]), show spectral indications of hydration on their surfaces. Absorption features at $\sim 3.0 \mu\text{m}$ are particularly indicative of aqueous alteration. These absorptions are likely due to hydroxyl and/or water-bearing materials (OH/H₂O) (e.g., [5], [6]), but could also be due to surficial OH implanted from solar wind or exogenic sources like those seen on Vesta [7]. We are observing and studying 60 new water-rich asteroids in the 3- μm region using NASA Infrared Telescope Facility (IRTF) and Gemini North telescopes, in addition to the 50 water-rich asteroids previously observed by [6] and [8]. We are also studying additional carbonaceous chondrite meteorites (e.g., CI, CM, CO, CV, CR, CH, and CB) by measuring their 3- μm spectra under asteroid-like conditions to determine their mineralogical and spectral indicators. Applying these spectral analyses of carbonaceous chondrites to water-rich asteroids in the 3- μm region has been challenging because chondrite spectra have generally been acquired in ambient terrestrial environments, and hence are contaminated by atmospheric water. In this work, however, chondrite IR reflectance spectra are measured under asteroid-like conditions (i.e., vacuum and elevated temperatures) to eliminate the adsorbed water that affected previous analyses. This investigation is important for matching the observed water-rich asteroids to specific chondritic groups for better understanding of the origin and evolution of our Solar System. Results from this work will also help analyze and characterize the returned carbonaceous samples from asteroids Bennu (OSIRIS-REx's target) and Ryugu (Hayabusa2's target), putting these returned samples into a wider perspective and broader Solar System context.

Methodology: Ground-based spectra of water-rich asteroids were measured using the long wavelength cross-dispersed (LXD: 1.9-4.2 μm) mode of the SpeX spectrograph/imager at the NASA IRTF and the cross-dispersed mode of the Near InfraRed Spectrograph (GNIRS) spectrometer at Gemini North, following the methodology of [6]. New 3- μm bi-directional reflectance spectra (*incidence* = 15°, *emission* = 45°, *phase angle* = 60°) of carbonaceous chondrites (CVs, COs, and CIs) have been collected at the Johns Hopkins University Applied Physics Laboratory (JHU APL) under vacuum-desiccated conditions, following the methodology used in [9].

Results: [8] found that CM (and CI) chondrites are possibly the meteorite analogs for water-rich asteroids with the sharp 3- μm band, attributed to phyllosilicates. The sharp

spectral group contains asteroids that are located in the $2.5 < a < 3.3$ AU region. No meteorite match was found by [8] either for the rounded group, Ceres-like group, or asteroid Europa-like group. These three spectral groups are located farther from the Sun ($3.0 < a < 4.0$ AU). Here we present new 3- μm spectra of water-rich asteroids, including 212 Medea, 690 Wratislavia, 372 Palma, 259 Aletheia, 114 Kassandra, 701 Oriola, 360 Carlova, 747 Winchester, 386 Siegena, 356 Liguria 233 Asterope, 135 Hertha, 87 Sylvania, and 142 Polana. Asteroid Polana, which is the main asteroid in the New Polana Family [10], is thought to be the probable source of primitive near-Earth asteroids including Benu and Ryugu [11]. The new 3- μm spectra are grouped according to the classification scheme of [6]. We will also present new 3- μm spectra of carbonaceous chondrites, which will be used to interpret ground-based, and eventually space-based, spectra of water-rich asteroids. We will then compare the new spectra of meteorites and asteroids to determine new possible matches on the basis of the 3- μm band.

References: [1] Clark (2009) *Science* 5952:552. [2] Pieters et al. (2009) *Science* 5952:568. [3] Sunshine et al. (2009) 5952:565. [4] Takir et al. (2017) *ApJ* 153:1. [5] Rivkin et al. (2002) In *Univ. Of Arizona Asteroids III* 235- 253. [6] Takir and Emery (2012) *Icarus* 219:641-654. [7] Reddy et al. (2012) *Icarus* 221:544-559. [8] Takir et al. (2015) 257:185-193. [9] Takir et al. (2013) 48:1618-1637. [10] Walsh et al. (2013) *Icarus* 225:283-297. [11] Bottke et al. (2015) *Icarus* 247:191-217.

Hayabusa2 landing site selection (LSS) training: Summary report of scientific evaluation

Hikaru Yabuta¹, Naru Hirata², Rie Honda³, Yoshiaki Ishihara⁴, Kohei Kitazato², Mutsumi Komatsu⁵, Akira Miura⁴, Koji Matsumoto⁶, Tomokatsu Morota⁷, Tomoki Nakamura⁸, Aiko Nakato⁹, Takaaki Noguchi¹⁰, Tatsuaki Okada⁴, Naoya Sakatani¹¹, Seiji Sugita¹², Shogo Tachibana¹², Satoshi Tanaka⁴, Eri Tatsumi¹², Sei-ichiro Watanabe⁷, Tomohiro Yamaguchi⁴, Yukio Yamamoto⁴, LSS, AA Team (Hayabusa2 Project)

¹Hiroshima University, ²University of Aizu, ³Kochi University, ⁴ISAS/JAXA, ⁵Sokendai, ⁶NAOJ, ⁷Nagoya University, ⁸Tohoku University, ⁹Kyoto University, ¹⁰Kyushu University, ¹¹Meiji University, ¹²Tokyo University

The Japanese C-type asteroid sample return mission, Hayabusa2, was launched on December 3, 2014. The spacecraft is scheduled to arrive at the near Earth asteroid Ryugu on July 2018. During its 18-month stay, remote-sensing observations will be carried out by the on-board instruments, Optical Navigation Camera (ONC), Near Infrared Spectrometer (NIRS3), Thermal Infrared Imager (TIR), and Light Detection and Ranging (LIDAR). Based on the observation data, the collection of the asteroid samples from three sites at maximum will be performed. We will carry out the landing site selection (LSS) within a month after the arrival to Ryugu, for the first touch down and for the release of MASCOT, a small hopping rover developed by DLR and CNES on October 2018.

It is therefore very important that scientists from remote sensing, MASCOT, and sample analyses are mingled to work out a landing site selection strategy by sharing the common picture of the multi-scale asteroid science. During this June-August 2017, we carried out the LSS training by using the asteroid Ryugu analog model “Ryugoid”. Beginning of shape modeling, the data products such as surface temperature, thermal inertia, grain sizes, visible and near infrared spectra, and spectral parameters (albedo, UV slope) were obtained from the Box A (at 20 km in altitude), Box C and mid-altitude (at 5 km in altitude) observations by TIR, ONC, NIRS3, and LIDAR teams. Then, six potential landing sites (zones A, B, C, D, D2, and E, in figure) were indicated by the system side. Based on the products, scientific evaluations (e.g., compositions and distributions of hydrate minerals, relative abundance of organic carbon, thermal metamorphism degree, space weathering degree, and number density of boulders) of these zones were conducted in order to prioritize the first landing site. This training has made us prepare for the actual LSS next year, to determine the most scientifically valuable site, that is, water-rich region.

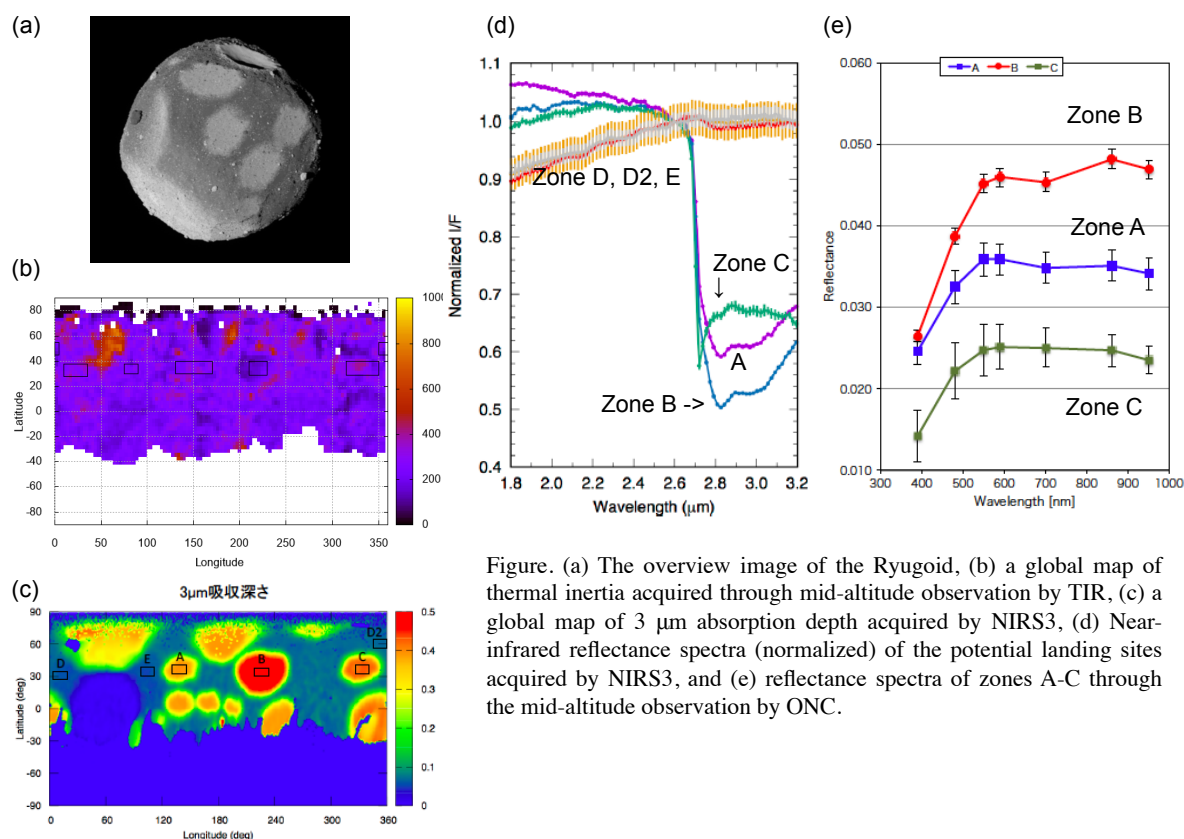


Figure. (a) The overview image of the Ryugoid, (b) a global map of thermal inertia acquired through mid-altitude observation by TIR, (c) a global map of 3 μm absorption depth acquired by NIRS3, (d) Near-infrared reflectance spectra (normalized) of the potential landing sites acquired by NIRS3, and (e) reflectance spectra of zones A-C through the mid-altitude observation by ONC.

Measuring Shock Stage of Itokawa Regolith Grains by Electron Back-Scattered Diffraction and Synchrotron X-ray Diffraction

Michael Zolensky¹, Takashi Mikouchi², Kenji Hagiya³, Kazumasa Ohsumi⁴, James Martinez¹, Kenji Hagiya³, Scott Sitzman⁵, Yasuko Terada⁴, Naoto Yagi⁴, Mutsumi Komatsu⁶, Hikaru Ozawa³, Yuta Taki³, Yuta Yamatsuta³, Atsushi Takenouchi², Hikari Hasegawa², Haruka Ono², Kotaro Higashi², Masaki Takata⁴, Arashi Hirata³, Ayaka Kurokawa³, Shoki Yamaguchi³.
¹ARES, NASA JSC, Houston, TX (USA); ²School of Science, Univ. of Tokyo (Japan); ³Graduate School of Life Science, Univ. of Hyogo (Japan); ⁴Japan Synchrotron Radiation Research Institute (Japan); ⁵Aerospace Corporation, El Segundo, CA, (USA); ⁶SOKENDAI (Japan).

We have been analyzing Itokawa samples in order to definitively establish the degree of shock experienced by the regolith of asteroid Itokawa, and to devise a bridge between shock determinations by standard light optical petrography, crystal structures as determined by electron and X-ray diffraction techniques [1,2,3,4]. We are making measurements of olivine crystal structures and using these to elucidate critical regolith impact processes. We use electron back-scattered diffraction (EBSD) and synchrotron X-ray diffraction (SXR). We are comparing the Itokawa samples to L and LL chondrite meteorites chosen to span the shock scale experienced by Itokawa, specifically Chainpur (LL3.4, Shock Stage 1), Semarkona (LL3.00, S2), Kilabo (LL6, S3), NWA100 (L6, S4) and Chelyabinsk (LL5, S4). In SXR we measure the line broadening of olivine reflections as a measure of shock stage. In this presentation we concentrate on the EBSD work. We employed JSC's Supra 55 variable pressure FEG-SEM and Bruker EBSD system. We are not seeking actual strain values, but rather indirect strain-related measurements such as extent of intra-grain lattice rotation, and determining whether shock state "standards" (meteorite samples of accepted shock state, and appropriate small grain size) show strain measurements that may be statistically differentiated, using a sampling of particles (number and size range) typical of asteroid regoliths.

Using our system we determined that a column pressure of 9 Pa and no C-coating on the sample was optimal. We varied camera exposure time and gain to optimize mapping performance, concluding that 320x240 pattern pixilation, frame averaging of 3, 15 kV, and low extractor voltage yielded an acceptable balance of hit rate (>90%), speed (11 fps) and map quality using an exposure time of 30 ms (gain 650). We found that there was no strong effect of step size on Grain Orientation Spread (GOS) and Grain Reference Orientation Deviation angle (GROD-a) distribution; there was some effect on grain average Kernel Average Misorientation (KAM) (reduced with smaller step size for the same grain), as expected. We monitored GOS, Maximum Orientation Spread (MOS) and GROD-a differences between whole olivine grains and sub-sampled areas, and found that there were significant differences between the whole grain dataset and subsets, as well as between subsets, likely due to sampling-related "noise". Also, in general (and logically) whole grains exhibit greater degrees of cumulative lattice rotation. Sampling size affects the *apparent* strain character of the grain, at least as measured by GOS, MOS and GROD-a. There were differences in the distribution frequencies of GOS and MOS between shock stages, and in plots of MOS and GOS vs. grain diameter. These results are generally consistent with those reported this year [5]. However, it is unknown whether the differences between samples of different shock states exceeds the clustering of these values to the extent that shock stage determinations can still be made with confidence. We are investigating this by examination of meteorites with higher shock stage 4 to 5.

Our research will improve our understanding of how small, primitive solar system bodies formed and evolved, and improve understanding of the processes that determine the history and future of habitability of environments on other solar system bodies. The results will directly enrich the ongoing asteroid and comet exploration missions by NASA and JAXA, and broaden our understanding of the origin and evolution of small bodies in the early solar system, and elucidate the nature of asteroid and comet regolith.

References: [1] Zolensky et al. (2012) *Lunar and Planetary Science*, XLIII, #1477, Lunar Planet. Inst., Houston (CD-ROM); [2] Zolensky et al. (2014) *Hayabusa 2014: 2nd Symposium of Solar System Materials. Abstracts.*; [3] Zolensky et al. (2016) *Hayabusa 2016 Abstracts*; [4] Hagiya et al. (2016) *Abstracts, 79th Annual Meeting of the Meteoritical Society*; Ruzicka and Hugo (2017) *80th Annual Meeting of the Meteoritical Society*, 6368.

Transmission Electron Microscopy of Plagioclase-Rich Itokawa Grains: Space Weathering Effects and Solar Flare Track Exposure Ages.

Lindsay P. Keller¹ and Eve L. Berger²

¹*ARES, Code XI3, NASA/JSC, Houston, TX 77058*

²*GCS – Jacobs JETS – NASA/JSC, Houston, TX 77058.*

Introduction

Limited samples are available for the study of space weathering effects on airless bodies. The grains returned by the Hayabusa mission to asteroid 25143 Itokawa provide the only samples currently available to study space weathering of ordinary chondrite regolith. We have previously studied olivine-rich Itokawa grains and documented their surface alteration and exposure ages based on the observed density of solar flare particle tracks. Here we focus on the rarer Itokawa plagioclase grains, in order to allow comparisons between Itokawa and lunar soil plagioclase grains for which an extensive data set exists [1].

Samples and Methods

Four plagioclase-bearing grains from the JAXA collection were allocated for this study: RB-QD04-0058, RB-QD04-0074, RB-QD04-0090, and RA-QD02-0157. We embedded the particles in low viscosity epoxy and used an ultramicrotome to partly section three of the particles, placing the sections on TEM grids with continuous amorphous carbon support films. Sectioning of the fourth particle is underway. For two of the particles, the epoxy surrounding the particle was trimmed away on three sides to enable further sectioning utilizing a focused ion beam (FIB) instrument [2] (FEI Quanta 3D). The microtome and FIB sections were analyzed in a JEOL 2500SE scanning and transmission electron microscope (STEM) equipped with an energy-dispersive x-ray (EDX) spectrometer optimized for nanometer-scale quantitative x-ray mapping. Brightfield and darkfield images were acquired using both conventional TEM and STEM imaging. Solar flare particle tracks were imaged in STEM mode, and observed track densities were converted to apparent surface exposure ages using our recent calibration [3].

Results and Discussion

RB-QD04-0090 is an angular ~ 40 μm grain of twinned albitic plagioclase. No shock features are observed. EDX analyses give a composition of $\text{Ab}_{85}\text{Or}_{5}\text{An}_{12}$. Solar flare particle tracks occur with a density of $\sim 5 \times 10^9$ cm^{-2} which indicates a surface exposure of $\sim 110,000$ y (Figure 2). The particle is surrounded by a thin continuous amorphous rim ~ 50 nm wide. Quantitative EDX mapping shows that the rim consists of two layers, an inner amorphous layer ~ 20 nm thick with the same composition as the underlying crystal-line host, and an outer amorphous layer ~ 30 nm thick that is Fe-rich and compositionally distinct from the underlying layer and host grain (Figure 1). We interpret the inner layer as a solar wind amorphized layer, and the outer layer as a vapor deposit. Vapor deposits of this thickness are unusual for Itokawa grains, because most grains are typically dominated by solar wind damage [1, 3, 4]. Nanophase Fe grains are present as a thin outermost layer. A few adhering grains (also plagioclase) are attached to the grain surface. In addition, there are numerous ~ 0.1 - 0.3 μm crystals of NaCl on the grain surface. We also observed a thin continuous rim of NaCl surrounding the grain.

RB-QD04-0074 is an ~ 32 μm irregularly-shaped polymineralic grain. The grain contains major olivine (Fo65), twinned albite ($\text{Ab}_{85}\text{Or}_{2}\text{An}_{12}$), and minor orthopyroxene ($\text{En}_{65}\text{Fs}_{33}\text{Wo}_2$). The olivine and orthopyroxene are more Fe-rich than typical Itokawa grains [5] but consistent with literature data for LL chondrites [6]. The orthopyroxene contains a high density of stacking faults and the olivine contains numerous planar dislocations along (100). The planar dislocations in the olivine grain are consistent with those that develop due to moderate shock. The observed track density 6×10^7 cm^{-2} (corresponding to counting 6 tracks in 10 μm^2) is very low and is approaching the limit that can be reliably counted in a grain this large by TEM methods. The track density implies a short surface exposure of ~ 2000 y. The plagioclase shows a solar wind amorphized outer layer ~ 10 nm wide. The olivine grain appears undamaged and does not show a nanocrystalline solar wind damaged rim like those on olivine-rich Itokawa grains [7]. RB-QD04-0074 is over an order of magnitude younger than the other olivine and plagioclase grains we have analyzed and was either freshly excavated from greater depth in the Itokawa regolith, or possibly had an origin as a relatively fresh fragment of a larger grain due to regolith gardening. This grain also shows surface adhering NaCl particles. We had not previously detected NaCl particles on previous Hayabusa samples analyzed in our lab. Noguchi et al. [8] detected NaCl and KCl particles on Itokawa grains but were unable to determine whether they were indigenous or possible contaminants.

RA-QD02-0157 is an angular ~38 μm grain dominated by albitic plagioclase and minor FeS and olivine. FIB sectioning is underway and here we report preliminary observations from ultramicrotome thin sections. The plagioclase shows twinning and is compositionally similar to the other albite grains in this study. We have not observed solar flare tracks in this particle to date, although there appears to be a thin amorphous layer (<10 nm) that likely represents solar wind damage. Analysis of a FIB section will provide a better constraint on exposure age of this grain. A small FeS grain adhering to the surface shows a damaged, outer layer consistent with our previous work on solar wind damaged sulfide grains in Itokawa samples.

Comparison to Lunar Plagioclase

We have previously established a relationship between the width of solar wind damaged rims on lunar plagioclase and olivine, and their surface exposure age based on solar flare particle track densities [1]. Although large compositional differences exist between the albitic Itokawa plagioclase grains and the dominantly Ca-rich plagioclase in lunar soils, the solar wind damaged rim widths in Itokawa grains follows the trend for lunar plagioclase. The Itokawa grains show space weathering features typical of immature lunar soil grains.

Conclusions

We analyzed the space weathering features on three Itokawa plagioclase-bearing grains. Particles RA-QD04-0074 and RA-QD02-0157 are relatively fresh with little surface modification from solar wind damage. The low track density for -0074 suggests a surface exposure age of ~2000y. Particle RA-QD04-0090 has a much longer surface exposure (~110,000 y) and corresponding surface alteration including a 30 nm thick vapor deposit overlying a solar wind damaged layer.

References

[1] Keller, L. P. et al. (2016) LPSC 47, #2525. [2] Berger, E. L. & Keller, L. P. (2015) Microscopy Today 23, 18-23. [3] Berger, E. L. & Keller, L. P. (2015) LPSC 46, #2351. [4] Noguchi, T. et al. (2014) MAPS 49, 188. [5] Nakamura, T., et al. Science 333, 1113-1116. [6] Nakamura, T., et al. LPSC XXXXII, 1766. [7] Keller, L. P. & Berger, E. L. Earth, Planets and Space 66, 71-77. [8] Noguchi, T., et al. (2014) MAPS 49, 1305-1314.

Acknowledgement

We thank JAXA for allocating the particles analyzed in this study. This work was supported by a NASA LARS grant (LPK).

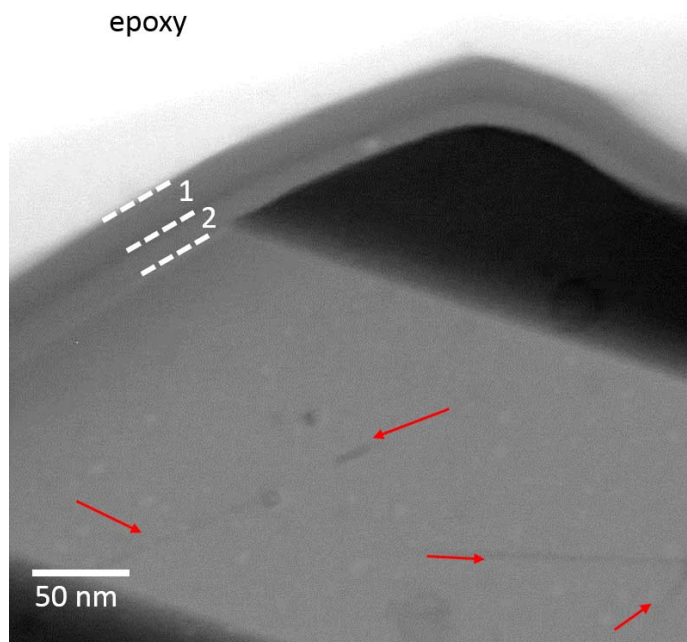


Figure 1. A brightfield STEM image from a FIB section of particle RA-QD04-0090 showing twinning in the host grain, solar flare particle tracks (red arrows), and a space-weathered rim consisting of two distinct layers, a vapor-deposited layer (1) and a solar wind damaged layer (2).

Microstructures of iron sulfide of Itokawa particles

T. Matsumoto¹, A. Miyake³, S. Nakao², A. Tsuchiyama³, M. Sakai²

¹Institute of Space and Astronautical Science, Japan Aerospace Exploration Agency (JAXA), ²Institute of Molecular Science, ³Kyoto University

(E-mail: tmatsumoto@planeta.sci.isas.jaxa.jp).

Introduction:

Space weathering has been referred to describe the collective processes that modify the optical properties, chemical compositions, and structures of materials on the surfaces of airless Solar System bodies [1]. Hayabusa spacecraft touched down to a S-type near-Earth asteroid 25143 Itokawa and recovered surface regolith particles, which are consistent with minerals contained in LL5-6 ordinary chondrite [2]. Analysis of Itokawa particles revealed nanoparticle-bearing rim, which are probably the major cause of alteration of reflectance spectra of Itokawa [3]. Prior to Hayabusa mission, the Near-Earth Asteroid Rendezvous (NEAR) mission's orbital study of S-type asteroid Eros revealed that change of reflectance spectra has been developing on Eros's surface similar to Itokawa's surface [4]. NEAR also discovered that Eros's surface appears to be strongly depleted in sulfur compared to ordinary chondrite [4]. However, sulfur depletion has not been obvious on Itokawa from remote-sensing observation and sample analysis so far. Sulfur in Itokawa samples is primarily bound in the form of iron sulfide [1], we investigated microstructures of iron sulfide of Itokawa particles in order to understand behavior of sulfur on airless bodies.

Experiments:

The four Itokawa particles were fixed with a 5 μm -diameter carbon fiber using glycol phthalate. The surface morphologies of the Itokawa particles were observed using a field-emission scanning electron microscope (Hitachi, SU6600) equipped with an energy-dispersive X-ray (EDX) spectroscopic detector (Bluker XFlash FladQUAD 5060FQ) at the Institute of Molecular Science, Japan. Regions of interest (ROI) were selected based on the FE-SEM observation, and electron-transparent sections including particle surface were prepared from the ROI using a focused ion beam (FEI, Helios G3 CX) at Kyoto University, Japan. The sections were observed using a field-emission transmission electron microscope (JEOL, JEM-2100F) equipped with an EDX system (JED-2300T) at Kyoto University.

Results:

Iron sulfides are visible as inclusions of olivine grains, adhered particles, and melt-splashes on the Itokawa particles. From surface observation using FE-SEM, we found needle-like structures protruding from the iron sulfide surfaces (Fig.1ab). The lengths of the needles range from several tenth nm to 1 μm . The needles often develop on porous iron sulfide surfaces (Fig.1ab). SEM-EDX analysis shows that the needles are composed of iron and they are deficient in sulfur (Fig.1c). The needles often contain minor nickel. So far, we lifted out FIB sections from a melt-splash of iron sulfide where needle-like structures develop on its surface. The melt-splash is an immiscible mixture of silicate and iron sulfide, covering an olivine grain. Fig. 1 shows a cross section of the melt splash of 50 nm in thickness including the needles. Elemental maps by TEM-EDX analysis clearly shows that the needle consists of iron and lacks in sulfur (Fig.1d). A TEM-selected area electron diffraction (SAED) pattern of the needle (Fig. 1f) indicates that the needle has a structure of body-centered cubic iron (α -iron). The iron sulfide layer is composed of amorphous structures, except for regions nearby the iron needle. Crystalline pyrrhotite structure is developed in the vicinity of the iron needle. Beneath the iron sulfide layer, vesicular damage rims are developed on olivine surface, which might have been formed due to the implantation of solar wind hydrogen and helium [3]. The existence of vesicular rim indicates that olivine surface has been exposed to the sun over a period of time, before the melt splash attached to the olivine surface.

Discussions:

Remarkable surface morphology of iron sulfide such as iron needles have not been reported in previous analysis of Itokawa particles. On the other hand, prior observation of pyrrhotite grain of Itokawa particles reported that the outer 10-nm-wide zone is sulfur-depleted, including metallic iron grains (<5 nm) [5]. Mineral surfaces exposed to the space environment can be modified through space weathering by solar wind irradiation and impacts of micrometeorites. In previous studies, the feasibility of alteration of iron sulfide by space weathering effects have been examined experimentally [6, 7]. Laboratory studies on the chemical alteration of troilite by 4keV He ions simulating exposure to the solar wind and by nanosecond laser pulses simulating evaporation by micrometeorite impact showed that sulfur is depleted from troilite by these both effects [6] and iron layer of 2-3 nm in thick is identified after He ion implantation [7]. However, these experiments have not produced metallic iron needles as observed in this study. Prior experiments of heating troilite at near its eutectic temperature under H₂ gas flow showed that sulfur evaporates from troilite and iron residue is formed through incongruent evaporation [8]. This experiment showed that iron exists as irregular rods or sheet of micron meter in size. This could suggest that heating events such as meteoroid impacts together with implantation of solar wind hydrogen cause metallic iron needles on iron sulfide of Itokawa particles.

These heating events and ion implantation may lead to preferential loss of sulfur from Itokawa. X-ray fluorescence observations of Itokawa by the Hayabusa spacecraft did not find evidence for a large sulfur depletion on this S-class asteroid, as seen on Eros, though errors are large due to low solar activity during the orbital phases of the Hayabusa mission [9]. The microstructures of iron sulfide observed in this study could suggest that sulfur depletion processes are ongoing on Itokawa.

References:

[1] Pieters. et al. 2000. *MAPS*, 35, 1101-1107 [2] Nakamura et al. (2011) *Science*, 333, 1113-1116. [3] Noguchi et al. (2014) *MAPS*, 49, 188–214. [4] Trombka et al. 2000. *Science*, 289, 2101-2105. [5] Keller and Berger. 2014. *EPS*, 66:71. [6] Loeffler et

al. 2008. *Icarus*, 195, 622-629. [7] Keller et al. 2010. *LPSC Abstract#1172*. [8] Tachibana and Tsuchiyama. 1998. *GCA*, 62, 2005-2022. [9] Arai et al. 2008. *EPS* 60:21-31.

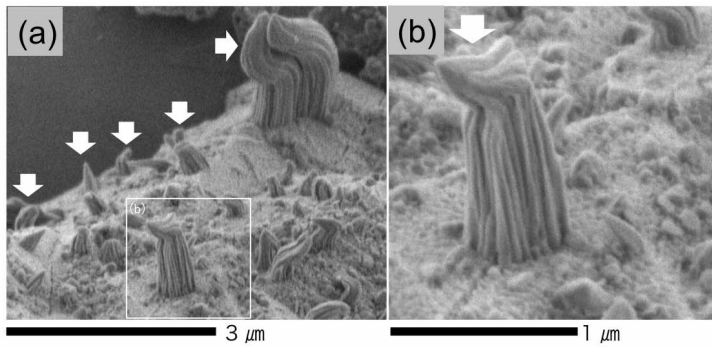
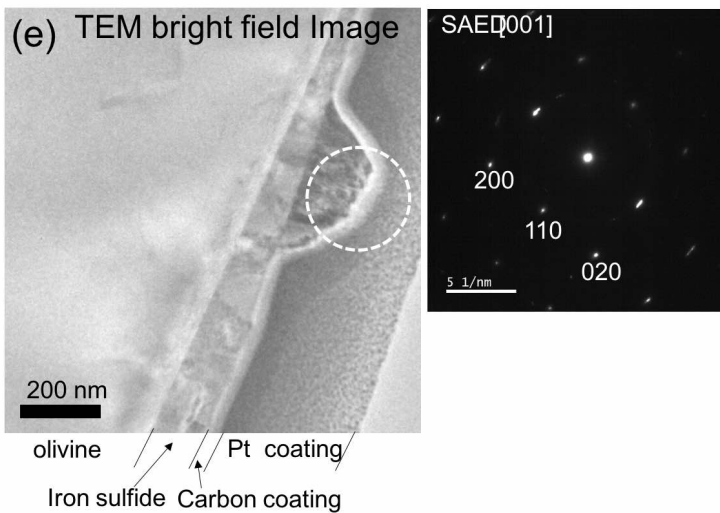
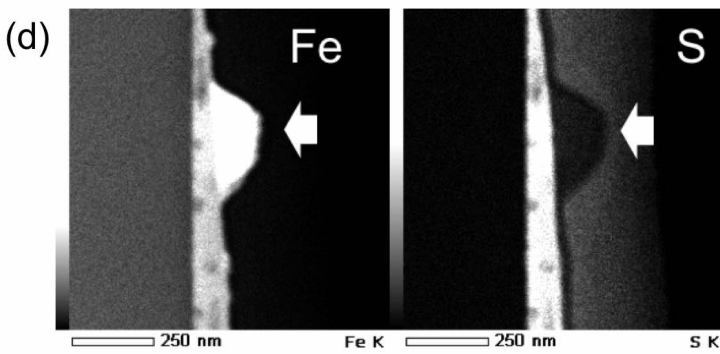
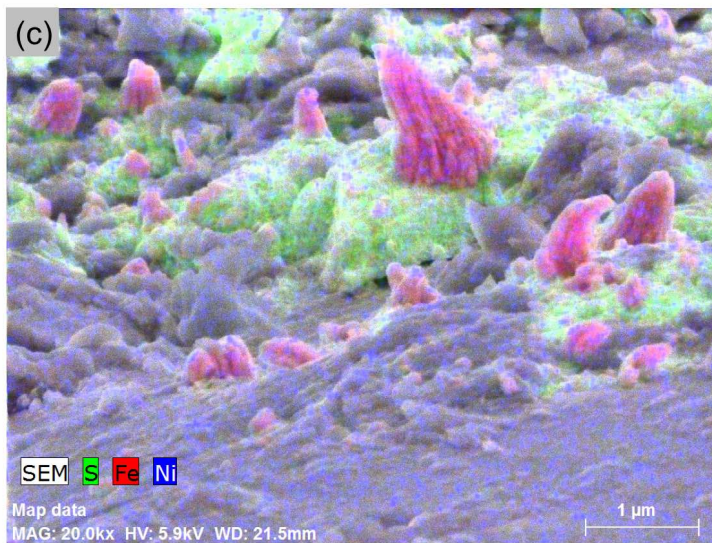


Figure 1 (a) (b) Secondary electron images of iron sulfide. Needle-like structures are indicated by arrows. (c) A SEM-EDX image of iron sulfide grains on olivine surfaces. (d) STEM-EDX images of a cross section of splash melt on olivine particle. A needle-like structure is indicated by arrows. (e) A TEM image and A SAED pattern of a needle-like structure.



FTIR Micro-tomography of five Itokawa Particles

Dionnet Z.¹, Aléon-Toppani A.¹, Borondics F.², Brunetto R.¹, Buellet A.C.¹, Djouadi Z.¹, King A.³ and Rubino S.¹

¹ *Institut d'Astrophysique Spatiale, CNRS, Université Paris-Saclay, CNRS*

² *SMIS beamline, Synchrotron SOLEIL, France*

³ *PSICHE beamline, Synchrotron SOLEIL, France*

Primitive extra-terrestrial materials (asteroidal and cometary particles, meteorites, IDPs) are characterized by a large mineralogical and compositional heterogeneity at different scales (from nm to mm) [1], which witnesses the complexity of the pre-accretional (solar nebula) and post-accretional (parent bodies) processes undergone by the small bodies of our solar system [2]. This heterogeneity has been observed by different techniques such as infrared (IR) micro spectroscopy mapping which is a powerful tool as it is (a) non-destructive and allows (b) comparison with astronomical observations of primitive Solar System small bodies (asteroids, comets, TNOs) [3] and (c) access both to the mineral and carbonaceous phases.

Thanks to Focal Plane Array (FPA) detector, 3D hyperspectral micro-tomography, can be performed to access structural information on intact samples [4, 5]. So far, this technique has never been applied to Hayabusa-1. Here, we will present the first 3D infrared reconstruction of five particles of Itokawa (RA-QD02-0214, RA-QD02-0223, RA-QD02-0232, RA-QD02-0156 and RB-QD04-0046). The FTIR micro analyses are performed at the SMIS beamline of the Synchrotron SOLEIL using a FPA detector with its Globar intern source. It is complementary to the X-ray micro-tomography previously performed on Hayabusa-1 particles [6]. Novel numerical methods have been developed to deal with a huge quantity of hyperspectral infrared data and we were able to obtain the 3D spatial distribution of chemical/mineralogical components (low/high calcium pyroxene, olivine, and plagioclase).

Another analysis was performed on grains of the Paris meteorite, one of the most primitive carbonaceous chondrite [7], to study the spatial correlation between the organic and mineral phases at scales down to $\sim 3 \mu\text{m}$. X-rays tomography was also performed on the same Paris particles, at the PSICHE beamline of the synchrotron SOLEIL, to obtain complementary information about the physical properties of the grains (shape, fractures, porosity ...). By combining X-ray and FTIR data we could obtain a physico-chemical description of precious grains in a non-destructive way and thus gives information about the formation and evolution of asteroids.

Performing FTIR micro-tomography on extraterrestrial samples rich in organic matter, is an important step in view of the sample return of dust particles from carbonaceous asteroid Ryugu by the Hayabusa-2 mission. In the sequence of analyses, micro-FTIR 3D spectral imaging coupled with X-rays tomography can provide a first, powerful non-destructive characterization of whole grains, in order to identify areas of interest and provide useful information before subsequent destructive analyses.

Acknowledgments

We are grateful to T.Yada and T.Nakamura for help and useful discussion. The micro-spectroscopy activities are supported by grants from Région Ile-de-France (DIM-ACAV) and SOLEIL.

References

- [1] Rietmeijer, F.J.M. 1998. *Reviews in Mineralogy*, 36, 95pp. (Chapter 2).
- [2] Alexander, C.M.O'D. 2007. *Geochimica et Cosmochimica Acta*, 71, Issue 17, p. 4380-4403.
- [3] Brunetto et al. 2011. *Icarus* 212, 896–910.
- [4] M.J. Nasse et al. 2011. *Nature method* 8, 1585.
- [5] M.C. Martin et al. 2013. *Nature Methods*, 10, 861–864.
- [6] Tsuchiyama A. et al. 2011. *Science* 333, 1125.
- [7] R. Hewins et al. 2014. *Geochimica et Cosmochimica acta* 124, 190-222.

Asteroid 25143 Itokawa Dust Particles: Mineralogy and Chondrite Affinities

Suporn Boonsue and John G. Spray

Planetary and Space Science Centre, University of New Brunswick, NB, E3B 5A3, Canada

In the third international announcement of opportunity (AO3) for Hayabusa mission sample investigation, we received three dust particle samples. Two specimens are polished sections of post-analyzed particles embedded in resin: RA-QD02-0011-02 (~30 μm) and RA-QD02-0048 (~20 μm) with Au- and C-coatings, respectively (Figure 1). The third sample is a pristine particle, RB-CV-0083 (~95 μm). Particle RA-QD02-0011-02 was originally described to be mainly composed of olivine, low-Ca pyroxene, high-Ca pyroxene, and plagioclase [1-4]. In this study, the morphology and composition of the particles were inspected by means of (1) field emission scanning electron microscopy (FESEM), and associated energy-dispersive X-ray microanalysis (EDS) and electron back-scattered diffraction (EBSD) using an Hitachi SU-70 with Schottky type field emission gun, and (2) micro-Raman spectrometry at the Planetary and Space Science Centre (PASSC), University of New Brunswick, Canada.

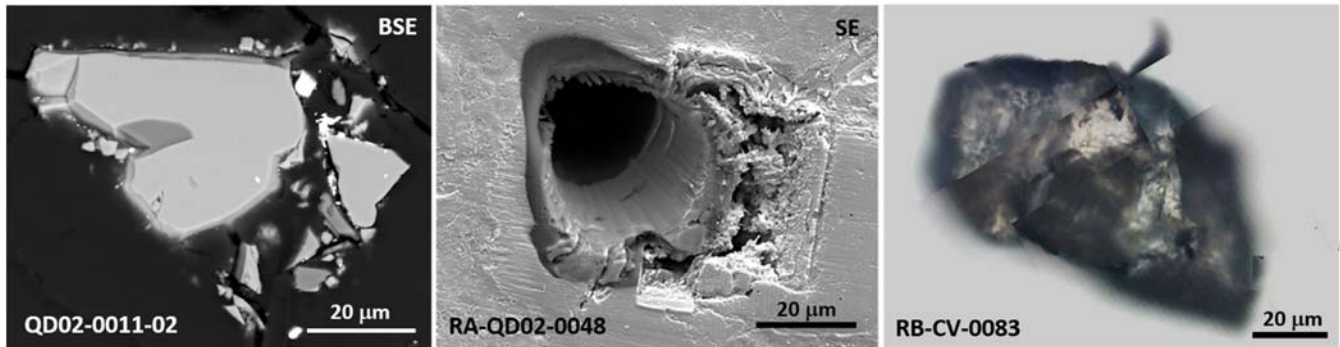


Figure 1. The three assigned Itokawa dust particles RA-QD02-0011-02 (~30 μm), RA-QD02-0048 (~20 μm), and RB-CV-0083 (~94 μm) provided by the Japan Aerospace Exploration Agency (JAXA) Hayabusa asteroidal sample return mission for this study.

The particles were collected from the surface of the S-type asteroid 25143 Itokawa. The particles comprise olivine, pyroxene and plagioclase. Fe-Ni metal, troilite (FeS), and chromite are also present. Energy dispersive spectrometry reveals that the olivine is Fo_{70} , and the plagioclase is $(\text{Ab}_{81}\text{An}_{13}\text{Or}_6)$. The plagioclase is interstitial to the olivine. The EBSD pattern of the $(\text{Mg,Fe})\text{SiO}_4$ phase in RA-QD02-0011-02 matches well with the pattern of the orthorhombic crystal structure of forsterite with space group *Pbmn*. The unit cell dimensions are $a = 4.76 \text{ \AA}$, $b = 10.21 \text{ \AA}$, $c = 5.98 \text{ \AA}$, $\alpha = 90.0^\circ$, $\beta = 90.0^\circ$, $\gamma = 90.0^\circ$ (Figure 2a). Raman analysis of the olivine reveals high intensity Raman bands at 819 and 851 cm^{-1} , with a Raman band calculated Fo number of 70 (Figure 3a). In addition, the $(\text{Na,K,Ca})(\text{AlSi})_4\text{O}_8$ phase next to olivine yields a typical EBSD pattern of amorphous material (Figure 2b). Raman analysis of the plagioclase reveals a broad band of amorphous material with an intense Raman band of crystalline phase albite/oligoclase. Both EBSD and the Raman results suggest that plagioclase was partially transformed to maskelynite (feldspathic glass). Intense Raman bands at 678, 659, 334 and 1006 cm^{-1} of orthopyroxene were obtained from RB-CV-0083. A cluster of forsterite ($\text{Fo}_{68.7}$), augite and plagioclase ($\text{Na}_{0.81}\text{Ca}_{0.12}\text{K}_{0.06}(\text{Al,Si})_4\text{O}_8$) present at the rim of the particle. A microcrystal (~5 μm diameter) of rounded, unzoned forsterite ($\text{Fo}_{69.5}$) with a nano-lath of albite/oligoclase (~1.0 $\mu\text{m} \times 500 \text{ nm}$) occurs in dust particle RB-CV-0083. The $\text{Mg}/(\text{Mg}+\text{Fe}+\text{Ca})$ ratio in pyroxene based on Raman band recalculation (678 and 334 cm^{-1}) is 0.7 (En_{70}) (Figure 3b), which is in good agreement with the EDS results ($\text{W}_{0.3}\text{En}_{7.3}\text{Fs}_{24}$). The olivine and orthopyroxene compositions are consistent with those of an LL4-6 chondrite. The presence of maskelynite suggests that the particles experienced shock metamorphism. The compositional homogeneity of olivine and the development of plagioclase indicate that the petrologic type of Itokawa dust particles is derived from a highly equilibrated chondrite. Our study confirms that the analyzed Itokawa dust particles are from a shocked equilibrated LL4-6 chondrite that now forms part of the asteroid's regolith. The source of the dust particles remains conjectural in that they could be from fragmented projectiles that impacted Itokawa, or from excavated material from within Itokawa, which itself is probably an assemblage of multiple asteroid components. The presence of maskelynite strongly suggests that the asteroid experienced shock impact during its evolution.

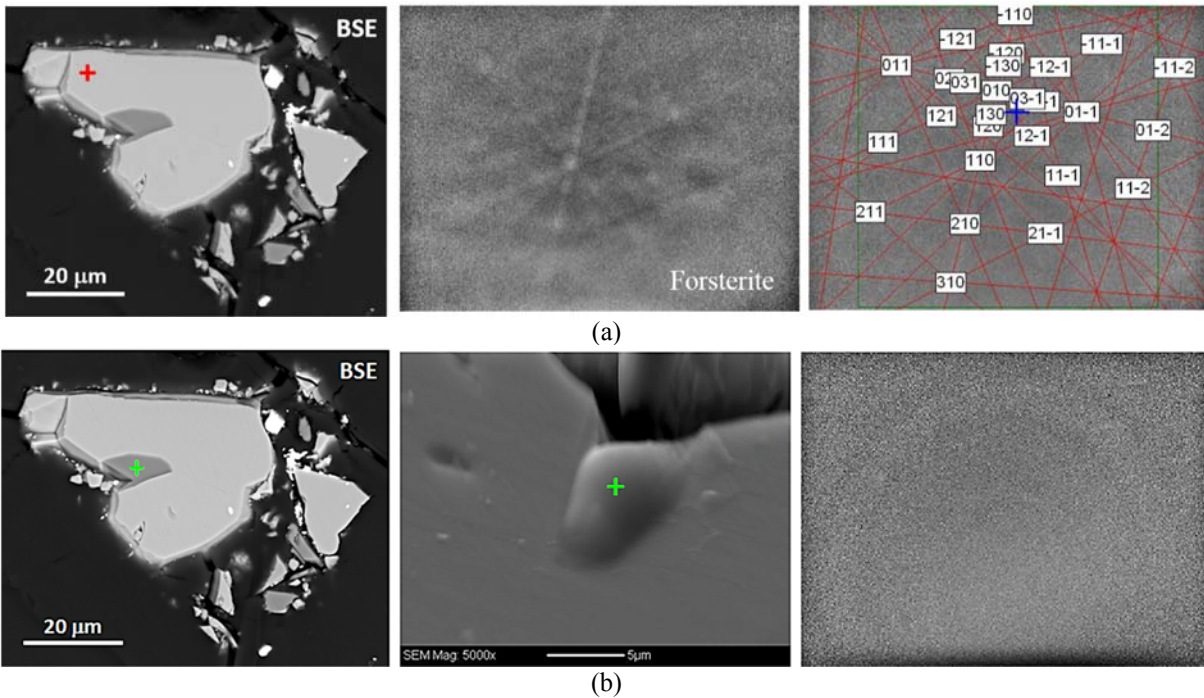


Figure 2. (a) The EBSD pattern of the (Mg,Fe)SiO₄ phase in RA-QD02-0011-02 matches well with the pattern of the orthorhombic crystal structure of forsterite (*Pbmm*) with unit cell dimensions $a = 4.76 \text{ \AA}$, $b = 10.21 \text{ \AA}$, $c = 5.98 \text{ \AA}$, $\alpha = 90.0^\circ$, $\beta = 90.0^\circ$, $\gamma = 90.0^\circ$. (b) Electron backscattered diffraction patterns (EBSD) of (Na,K,Ca)AlSi₃O₈ phases shows an amorphous EBSD diffraction pattern in the absence of Kikuchi bands.

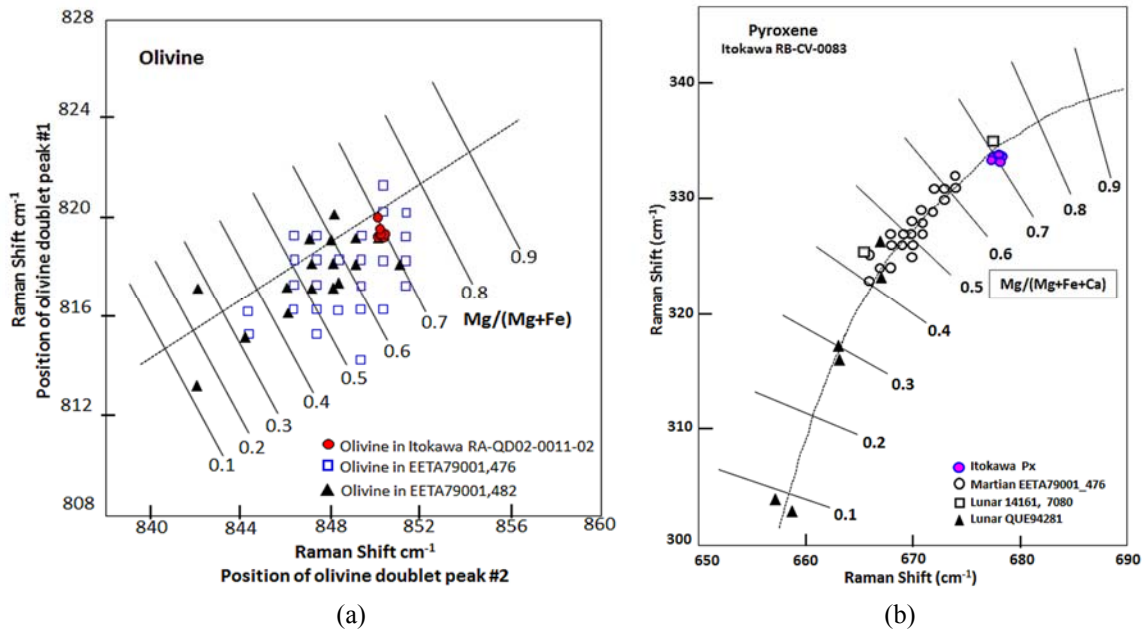


Figure 3. (a) The Raman peak positions at 851 and 819-820 cm^{-1} of olivine in Itokawa sample RA-QD02-0011-02 (red dots) are plotted on a diagram of peak positions of its characteristic Raman modes of olivine [5]. The data points fall along the calibration line suggesting the Mg/(Mg+Fe) value for the Itokawa olivine ~ 0.7 (Fo₆₅₋₇₀). (b) The data for a pair of peak positions of characteristic Raman modes (678 and 334 cm^{-1}) for orthopyroxene from RB-CV-0083 are plotted on the curve (pink dots), which corresponds to Mg/(Mg+Fe+Ca) molar fraction in pyroxene values of 0.7 (En₇₀) [6].

References

- [1] Yurimoto et al. 2011. Science. 333, 1116-1119. [2] Nakamura et al. 2011. Science 333, 1113-1116. [3] Tsuchiyama et al. 2011. Science. 333, 1125-1128. [4] Yada et al. 2012. Japan Aerospace Exploration Agency, Japan, unpublished document. [5] Wang et al., 2004. J. Raman Spectrosc. 35, 504-514 [6] Huang et al., 2000. Am. Mineralogist 85, 473-479.

Electrical properties of Itokawa grains returned by Hayabusa

F. Cipriani¹, N. Drozdovski¹, D. Koschny¹, L. Colangeli¹, M. Ferrari^{2,3}, V. Della Corte², M. Accolla^{2,3}, B. Butler¹, A. Rotundi^{2,3}, B.Shortt¹, S. Sanders¹, D. C.v.d. Luijt¹, D. Breeveld, ¹ ESA/ESTEC, Keplerlaan 1, 2200AG, Noordwijk, The Netherlands E-mail : fabrice.cipriani@esa.int ² INAF-Istituto di Astrofisica e Planetologia Spaziali, Via Fosso del Cavaliere 100, 00133 Roma, Italy ³ Dip. Scienze e Tecnologie, Universita degli Studi di Napoli "Parthenope", Centro Direzionale I C4, 80143 Napoli, Italy

Although a wealth of data exists on the properties of lunar regolith samples returned by Apollo missions e.g. [1,2] as well as investigations on terrestrial minerals, no such experimental data have yet been collected on asteroids material. In this study we present the measured secondary electron emission characteristics from areas of samples RA-QD02-0126-02 and RA-QD02-0136-14 [3] under electronic irradiation within the range 200eV to 5keV. Such measurements are related to surface structure, orientation and mineralogy, and compared to reference measurements including single grains and powders of reference materials of high purity, as well as terrestrial minerals and planetary analogs (see exemple Figure 1). In addition we observe the build-up of local electric field patterns arising from surface electrostatic charging in relation with grains morphology. Consequences on our understanding of regolith properties and electrostatic effects on planetary regolith will be discussed.

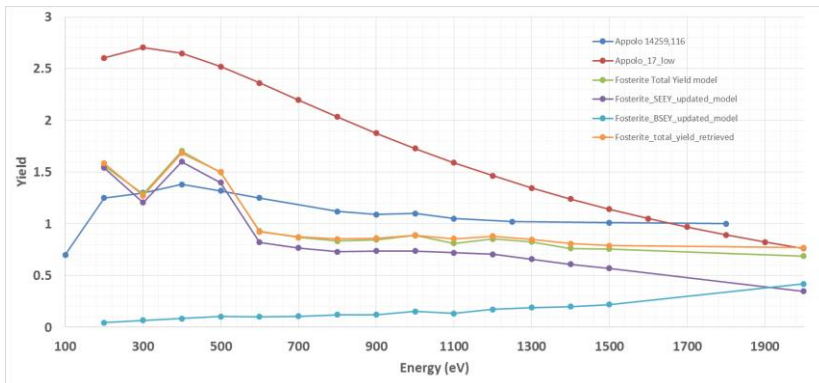


Figure 1: Secondary emission yields measured from Fosterite grains

References:

- [1] B. Feuerbacher et al , *Proceedings of the Third Lunar Science Conference*, 1972: Vol. 3, pp. 2655-2663
- [2] D.W. Strangway et al, *Earth and Planetary Science Letters*, 1972, Volume 16, Issue 2, pages 275-281,
- [3] Nakamura et al. , 2014, *Meteorit Planet Sci*, 49: 215–227. 10.1111/maps.12247

Particle track densities in olivine of the heated Jbilet Winselwan CM2 chondrite: Constraints on regolith heating?

Dennis Harries¹ and Philip Wild¹

¹*Institute of Geosciences, Friedrich Schiller University Jena, Carl-Zeiss-Promenade 10, 07745 Jena, Germany (Email: dennis.harries@uni-jena.de).*

Sample-return missions underway to the near-Earth objects 101955 Bennu (OSIRIS-REx) and 162173 Ryugu (Hayabusa 2) are expected to return surface regolith from two primitive C-group asteroids for laboratory study. Spectroscopically the C-group asteroids share similarities with CI and CM chondrites and are likely parent bodies of these meteorite groups. Material returned from the Moon and S-type asteroid 25143 Itokawa has shown that phenomena related to space weathering are well-recorded on the surface of silicate grains [1]. The degree (or maturity) of space weathering can potentially provide insights into the evolution of regoliths and, therefore, shed light on the dynamical evolution of near-Earth asteroids and their orbits [2,3,4]. Olivine is a good candidate for comparative taxonomy of space weathering due to its wide-spread occurrence in lunar and asteroidal samples and its experimentally extensively studied properties. If C-group asteroids are indeed related to CI and CM chondrites, olivine is expected to be a significant mineral in their regoliths. However, aqueous and thermal alteration processes recorded in CI and CM chondrites potentially leave morphological and chemical signatures on mineral surfaces, onto which space weathering would be superposed. This motivated us to investigate olivine grains of the Jbilet Winselwan (JW) meteorite, a moderately heated (tentatively <500 °C) CM2 chondrite [5]. In particular, we try to understand how olivine grains and the phyllosilicate mineralogy of JW can be used to constrain the heating event, which may have taken place in a number of different settings, e.g., deep in the CM2 parent body, in the regolith of a rubble-pile asteroid, or during the meteoroid stage of JW's travel towards the Earth.

Material and Methods: A 37.6 gram fragment of JW was sliced using a diamond wire saw and interior slices were used to produce two polished petrographic sections (~20×30 mm²) and cuboidal subsamples (~10×7×7 mm³). The cuboids were subjected to 100 to 150 cycles of freeze-thaw disaggregation in high-purity water. After drying, olivine crystals were separated by hand-picking and mounted onto SEM stubs or epoxy-embedded and polished. The grain mounts and polished petrographic sections were studied by field-emission SEM. The polished grain mounts were etched in WN solution in order to reveal damage tracks produced by ionizing, high-energy particles [6].

Results and Discussion: SEM imaging of the JW petrographic sections indicates subtle textural heterogeneities, most evident by variations in the abundance of serpentine/tochilinite-like aggregates. There is no obvious brecciation as seen in other CM2 chondrites [7] and specimens of JW [8]. Many components (dominantly chondrules) are surrounded by fine-grained rims, and the general texture resembles a primary accretionary rock [7]. The freeze-thaw disaggregated material is a black, non-cohesive powder (~80% <100 μm, ~50% <50 μm).

Euhedral to subhedral olivine crystals are optically prominent objects in the powder. The hand-picked olivine grains have median sizes of ~240 μm and a size range of 100 to 600 μm. Comparison with the petrographic sections suggests that the larger grains often occur as single grains within the meteorite. The smaller ones are most probably derived from porphyritic chondrules. The surface morphologies show a large diversity and can be subdivided into 'as-grown' crystal surfaces and fractured surfaces. Pristine surfaces are smooth and featureless, fresh fracture surfaces are typically characterized by step-like hackle marks. Altered surfaces have developed significant roughness through dissolution and the formation of secondary mineral scales. Such features superposed on surfaces with hackle marks suggest that fracturing had occasionally occurred before aqueous alteration.

We have studied a total of 81 olivine grains from three interior cuboids of JW for particle tracks, and etching has revealed tracks in 65 of them. In all cases the track densities are <5×10⁴ tracks/cm² (Fig. 1), and the median is ~9400 tracks/cm² (~6500 tracks/cm², if upper limit track densities for track-free grains are considered). The maximum track densities found in two grains are approximately consistent with the background track densities due to galactic cosmic rays (GCR) in typical CM2 chondrites [7]. However, the median values are much lower than typical GCR background track densities. The absence of brecciation and track-rich grains (>10⁶ tracks/cm², from irradiation by solar flare ions) indicates that the material of our JW specimen was never exposed in the upper few millimeters of a regolith. This is corroborated by the absence of solar wind noble gases in other samples of JW [9]. However, JW's unusually long Neon exposure age of 6.6±1.7 Ma [9] and the very low GCR track count suggests that GCR tracks may have been partially annealed by the, so far unidentified, heating event.

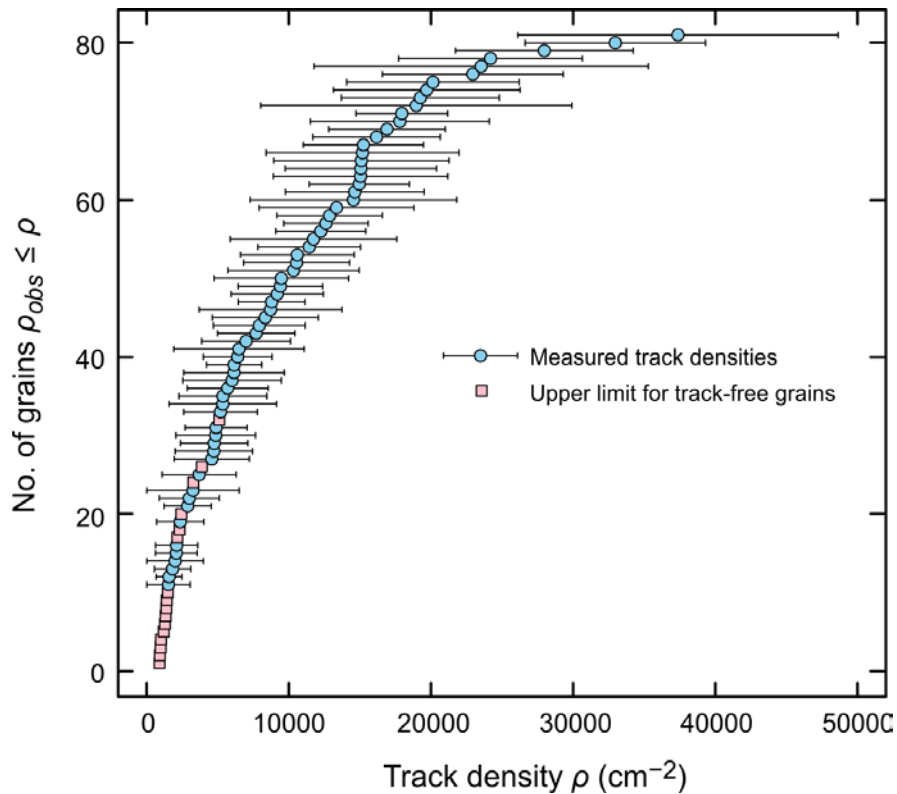


Figure 1. Cumulative plot of the particle track densities in Jbilet Winselwan olivines.

If JW was heated deep within its parent body, then GCR tracks and GCR-produced neon should have been acquired consistently during the meteoroid stage, unless the meteoroid that delivered JW to Earth was very large, and our specimen was deeply shielded within. The freshness of most JW specimens and the total known mass of JW meteorites of less than 10 kg (e.g., compared to >100 kg of Murchison) rule this possibility somewhat unlikely. Alternatively, JW may have been heated during a regolith residence or its meteoroid stage, e.g., by solar irradiation at low perihelion distances. If indeed solar heating can be made responsible for the mineralogical changes observed in JW (and possibly other heated CM and CM-like chondrites [10]), the implications for our understanding of space weathering phenomena in returned samples would be large, as heating and annealing may alter the exposure record of space-weathered grains (e.g., [3]).

References

- [1] Noguchi T. et al. (2011) *Science* 333:1121–1125. [2] Conolly H. C. et al. (2015) *Earth, Planets and Space* 67:12. [3] Harries D. and Langenhorst F. (2014) *Earth, Planets and Space* 66:163. [4] Harries D. et al. (2016) *Earth and Planetary Science Letters* 450:337–345. [5] Nakamura T. et al. (2014) *Antarctic Meteorites XXXVII*, 54. [6] Krishnaswami S. et al. (1971) *Science* 174:287–291. [7] Metzler K. (2004) *Meteoritics & Planetary Science*, 39:1307–1319. [8] Zolensky M. E. et al. (2016) 47th Lunar and Planetary Science Conference, abstract #2148. [9] Meier M. M. M. et al. (2016) *Meteoritics & Planetary Science* 51:A455. [10] Harries D. and Langenhorst F. (2013) *Meteoritics & Planetary Science* 48:879–903.

Acknowledgements

We acknowledge funding from Friedrich Schiller University Jena (DRM/2016-01). The SEM facility at U Jena is supported by the DFG (grant LA 830/14-1 to F. Langenhorst).

Carbon isotopic ratios of calcite grains in the LAP 031166 CM chondrite: Implications for possible link between CM and cometary ices.

Wataru Fujiya¹, Kohei Fukuda², Paula Lindgren³, Martin R. Lee⁴, Mizuho Koike⁵, and Yuji Sano⁵

¹Ibaraki University, 2-1-1 Mito, Bunkyo, Ibaraki 310-8512, JAPAN. (wateru.fujiya.sci@vc.ibaraki.ac.jp),

²University of Tokyo, ³Lund University, ⁴University of Glasgow, ⁵Atmosphere and Ocean Research Institute, University of Tokyo.

Introduction: Carbonate minerals are ubiquitous in CM chondrites, which formed by aqueous alteration in the CM chondrite parent body. Previous studies have shown that C isotopic ratios of CM carbonates are highly variable at whole-rock scales as well as among individual grains in single meteorites [e.g., 1-3]. Despite extensive studies on C isotopic ratios of CM carbonates, the reason for variability in $\delta^{13}\text{C}$ variation and the origin of the carbonate C remain poorly understood.

Here we report C isotopic ratios of calcite (CaCO_3) in the LAP 031166 CM chondrite (CM 2.1), and discuss the origin of the carbonate C and a possible link between ices in CMs and in comets. The O isotopic ratios of calcite in this meteorite were reported by Lindgren et al. [4].

Experimental: Carbon-isotope analysis was performed with the NanoSIMS 50 installed at Atmosphere and Ocean Research Institute, the University of Tokyo, on the calcite grains whose O isotopic ratios were measured previously. Negative secondary ions of $^{12}\text{C}^-$, $^{13}\text{C}^-$, $^{18}\text{O}^-$, $^{12}\text{C}^{14}\text{N}^-$, and $^{28}\text{Si}^-$ produced by rastering a Cs^+ primary ion beam (20-30 pA, $\sim 1 \mu\text{m}$ in diameter) over $6 \times 6 \mu\text{m}^2$ sized areas were detected simultaneously with five electron multipliers.

Results and discussion: The $\delta^{13}\text{C}_{\text{PDB}}$ and $\delta^{18}\text{O}_{\text{SMOW}}$ values of the calcite grains in LAP 031166 are shown in Fig. 1, together with literature data of Ca-carbonate (calcite and aragonite) in the Murchison, Nogoya, and Paris CM chondrites [3,5,6]. The $\delta^{13}\text{C}$ and $\delta^{18}\text{O}$ values of the CM carbonates are highly variable, ranging from ~ 20 to 80‰ and from ~ 15 to 40‰ , respectively, and they do not correlate with each other.

Alexander et al. [1] have suggested that the range in $\delta^{13}\text{C}$ can be explained by variable formation temperatures (0-130 °C) of CM carbonates which are isotopically equilibrated with gaseous C species dominated by CO (or CH_4). However, this model implies that the $\delta^{13}\text{C}$ and $\delta^{18}\text{O}$ values of the CM carbonates would correlate, which is clearly not the case as demonstrated by this work (Fig. 1). Instead, the observed $\delta^{13}\text{C}$ range must be produced under nearly constant temperatures.

Here we propose a modified version of the model outlined by Alexander et al. [1], where we consider mixing of CO_2 and CO gases with higher and lower $\delta^{13}\text{C}$ values, respectively. Because the equilibrium CO/CO_2 ratios are $\ll 1$ for f_{O_2} higher than the iron-magnetite buffer, CO should be converted to CO_2 and the CO/CO_2 ratios of gas phases would have decreased with time. As the CO/CO_2 ratios decreased, CO_2 as well as carbonates acquired lower $\delta^{13}\text{C}$ values. Given $1000\ln\alpha(\text{calcite}-\text{CO}_2)$ of ~ 10 -14 at 0-30 °C [7], where α is a C isotopic fractionation factor, the CM carbonates with the highest $\delta^{13}\text{C}$ values of $\sim 80\text{‰}$ were equilibrated with CO_2 with $\delta^{13}\text{C} \sim 70\text{‰}$. The $\delta^{13}\text{C}$ value of the trapped CO in Murchison is $\sim 30\text{‰}$ [8]. The lowest $\delta^{13}\text{C}$ values of the CM carbonates are ~ 20 -30‰, which is common for all the CM chondrites analyzed (Fig. 1). Therefore, the gaseous C species which coexisted with the CM carbonates with the lowest $\delta^{13}\text{C}$ values of ~ 20 -30‰ would have been dominated by CO_2 , i.e., most of CO was converted to CO_2 . If correct, the $\delta^{13}\text{C}$ value of the bulk gaseous C species ($\text{CO}_2 + \text{CO}$) would be $\sim 10\text{‰}$. Using the above numbers, mass balance calculation suggests that a CO/CO_2 mole ratio of the gaseous C species which coexisted with the CM carbonates with the highest $\delta^{13}\text{C}$ value of $\sim 80\text{‰}$ would be ~ 1.5 , which may reflect the CO/CO_2 ratio of ice accreted onto the CM parent body. The carbonate $\text{C}/\text{H}_2\text{O}$ mole ratios of most CMs range from ~ 0.01 to 0.1 [1]. These carbonate $\text{C}/\text{H}_2\text{O}$ ratios may set lower limits on the $\text{CO}_2/\text{H}_2\text{O}$ ratio of the CM ices because of possible CO_2 loss. Thus, CO_2 accounts for at least 1 % of the CM ices.

The inferred CO/CO_2 and $\text{CO}_2/\text{H}_2\text{O}$ mole ratios of the CM ices are shown in Fig. 2, together with those of cometary ices [9]. Unfortunately, only upper limits on the CO/CO_2 ratios are obtained for most of the observed comets. Nevertheless, the CO/CO_2 ratios of these comets seem lower than unity, and thus, lower than those of the CM ices. Although the possible similarity between ices in CMs and in some comets cannot be ruled out, these observations suggest that ices in the two classes of bodies had a different origin, which is consistent with contrasts in the D/H ratios of water between CMs and comets [10].

References: [1] Alexander C. M. O'D. et al. 2015. Meteorit. Planet. Sci. 50:810. [2] Tyra M. A. et al. 2012. Geochim. Cosmochim. Acta 77:383. [3] Fujiya W. et al. 2015. Geochim. Cosmochim. Acta 161:101. [4] Lindgren P. et al. 2017. Geochim. Cosmochim. Acta 204:240. [5] Fujiya W. et al. 2016. Abstract #1712. 47th LPSC. [6] Vacher L. G. et al. 2017. Geochim. Cosmochim. Acta 213:271. [7] Chacko T. et al. 2001. Rev. Mineral. Geochem. 43.1. [8] Yuen G. et al. 1984. Nature 307:252. [9] Ootsubo T. et al. 2012. Astrophys. J. 752:15. [10] Alexander C. M. O'D. et al. 2012. Science 337:721

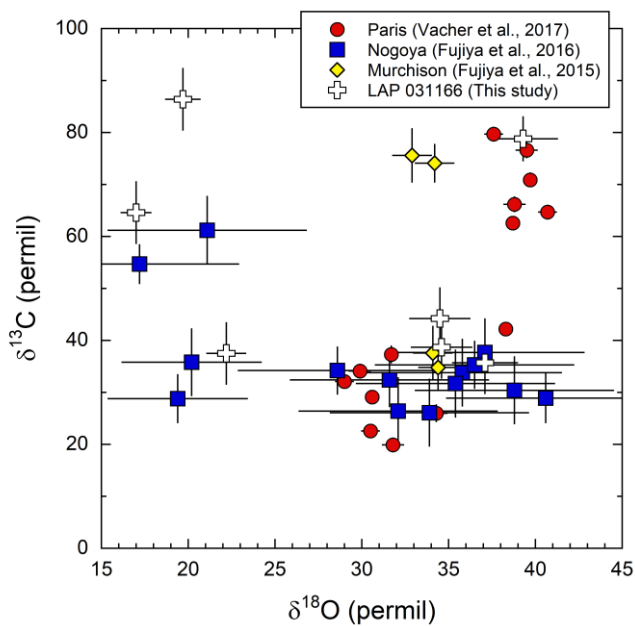


Fig. 1. $\delta^{13}\text{C}$ and $\delta^{18}\text{O}$ values of Ca-carbonates in CM chondrites. Errors are 2σ .

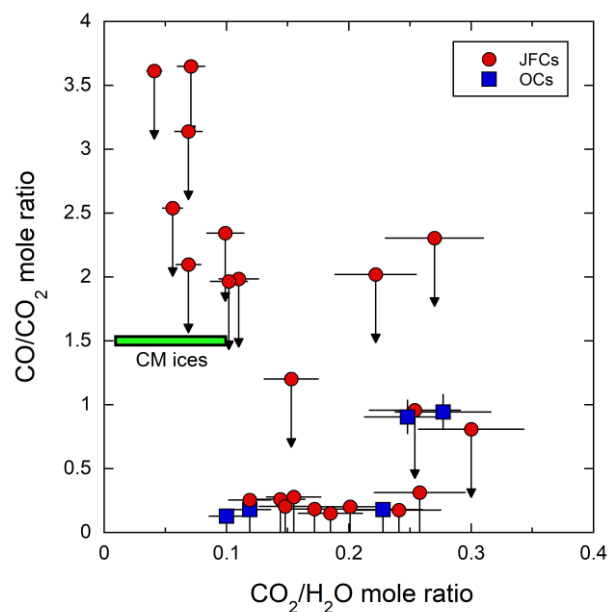


Fig. 2. CO/CO_2 and $\text{CO}_2/\text{H}_2\text{O}$ mole ratios of the inferred CM ices and comets. Data with arrows represent upper limits. JFCs: Jupiter-family comets, OCs: Oort cloud comets. Only comets which were observed within 2.5 AU from the Sun are shown, where H_2O effectively sublimates from the nucleus of the comet.

Volatile Contents in Vesicles in IDP Grains Analyzed with Scanning Transmission Electron Microscopy

Katherine D. Burgess¹, Rhonda M. Stroud¹, David Joswiack² and Donald Brownlee²

¹*U.S. Naval Research Laboratory, Washington, DC*

²*University of Washington, Seattle, WA*

Chondritic porous interplanetary dust particles (IDPs) are believed to come from comets and incorporate a wide variety of primitive early solar system and interstellar materials. Alteration is thought to be from nebular processes, such as solar wind exposure, and atmospheric entry heating. The compositional and structural changes associated with these processes can be analyzed using (scanning) transmission electron microscopy (S/TEM) with energy dispersive X-ray spectroscopy (EDS) and electron energy loss spectroscopy (EELS). Vesicles formed in the space weathered rims of grains are thought to be filled with hydrogen or helium from the solar wind, although heating may be required for the formation of the vesicles. Solar wind hydrogen has been identified in vesicles in the space weathered rim of a pyroxene grain [1], while helium was suggested as the likely source of bubbles formed in a pyrrhotite grain [2].

Stratospheric IDPs from collection plate U2012, flown on NASA Ames Research Center U2 aircraft in March 1993, were washed and embedded in epoxy, then microtomed and placed on grids for STEM analysis. The samples were baked at 140°C for six hours to drive off adsorbed water before insertion in the UHV system. Electron energy loss spectroscopy (EELS) and energy dispersive x-ray spectroscopy (EDS) data were collected with the NION UltraSTEM200-X at the U.S. Naval Research Laboratory, equipped with a Gatan Enfium ER EEL spectrometer and a Bruker SSD-EDS detector. The STEM was operated at 60 kV or 200 kV, with a ~0.1 nm probe. Spectra were collected as spectrum images (SI), with a spectrum collected for each pixel, allowing for mapping of variations in thickness and composition.

Sample U2012A-2J contains a pyrrhotite grain with a nominally continuous space weathered rim full of subhedral to euhedral vesicles. The voids range in size from a few nanometers to ~30 nm. Brownlee et al. [2] suggested that these voids formed due to helium implantation, but were unable to confirm the presence of helium in specific voids. High resolution EELS mapping of several of the voids reveals a small peak at ~22 eV associated with individual voids, indicating they are filled with helium from the solar wind (Figure 1).

A vesicular grain observed in sample U2012A-3C is much more enigmatic (Figure 2). The core of the grain is iron sulfide and it is surrounded by a highly vesicular oxygen-rich shell. EDS data show the rim material contains significant O, Fe and S, along with several at% Mg and trace (~0.5 at%) Si. EELS data from the vesicles show small peaks at 8.5 eV and ~13 eV, both associated with hydrogen [1]. Additionally, the carbon K-edge in spectra from the same vesicles shows a distinct peak at 287.4 eV due to the presence of C-H bonds. Attribution of this peak to a specific compound is ambiguous due to the ubiquity of these types of bonds in natural materials as well as laboratory sources. The peak is associated only with this particle and clearly tied to the individual vesicles, suggesting it is indigenous. A sharp peak at the same energy is seen in hexamethyl disiloxane [3], a compound related to the silicone oil in which the IDPs were collected, and hexane [4], used to wash the IDPs, both possible sources of contamination. However, the vesicles are not correlated with significant Si, as expected for silicone oil, and evidence of contamination is not seen elsewhere on the sample. Isotope measurements of the grain are planned in order to clarify the possible sources of the rim material and hydrocarbons.

The helium- and hydrogen-filled bubbles have very different morphologies, and it is unlikely the hydrogen filled vesicles formed solely due to the influence of the solar wind. The cores of both grains are predominantly iron sulfide. However, while the helium vesicles are euhedral and in material that otherwise very closely resembles vesicle-free portions of the grain, the hydrogen vesicles are in a highly porous rim that is rich in oxygen relative to the core of the grain and also has other minor and trace elements (e.g., Mg, Si) not present in the core. Solar wind helium-filled vesicles in lunar ilmenite are not euhedral [5], indicating that both host mineral composition and heating could play a role in vesicle formation and shape.

With the ability to identify and map the volatile contents of very small vesicles in IDPs and other extraterrestrial materials, we can better understand the timing of alteration and source of volatiles, whether from atmospheric heating and decomposition of

pyllosilicates, implantation by the solar wind, or contamination during collection and laboratory preparation procedures. This technique is applicable to samples collected from many airless bodies including Itokawa, Bennu, and Ryugu.

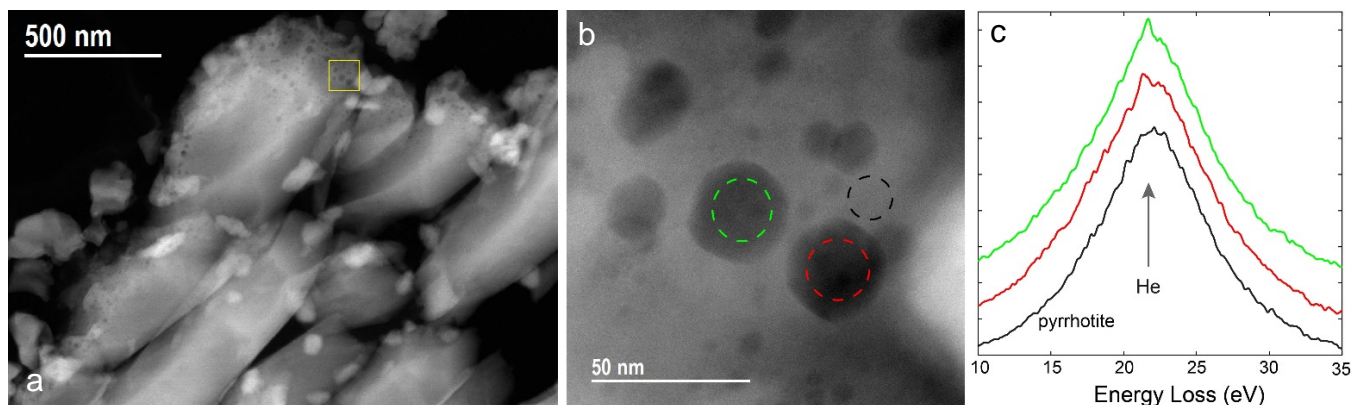


Figure 1. (a) HAADF image of pyrrhotite from U2012A-2J showing vesicle-rich rim around particle. (b) Higher magnification image of several euhedral vesicles. (c) EELS data from two vesicles indicated in (b) showing small peaks at ~ 22 eV indicating helium is present in the vesicles. A spectrum from a portion of the pyrrhotite not in a vesicle is shown for comparison (black).

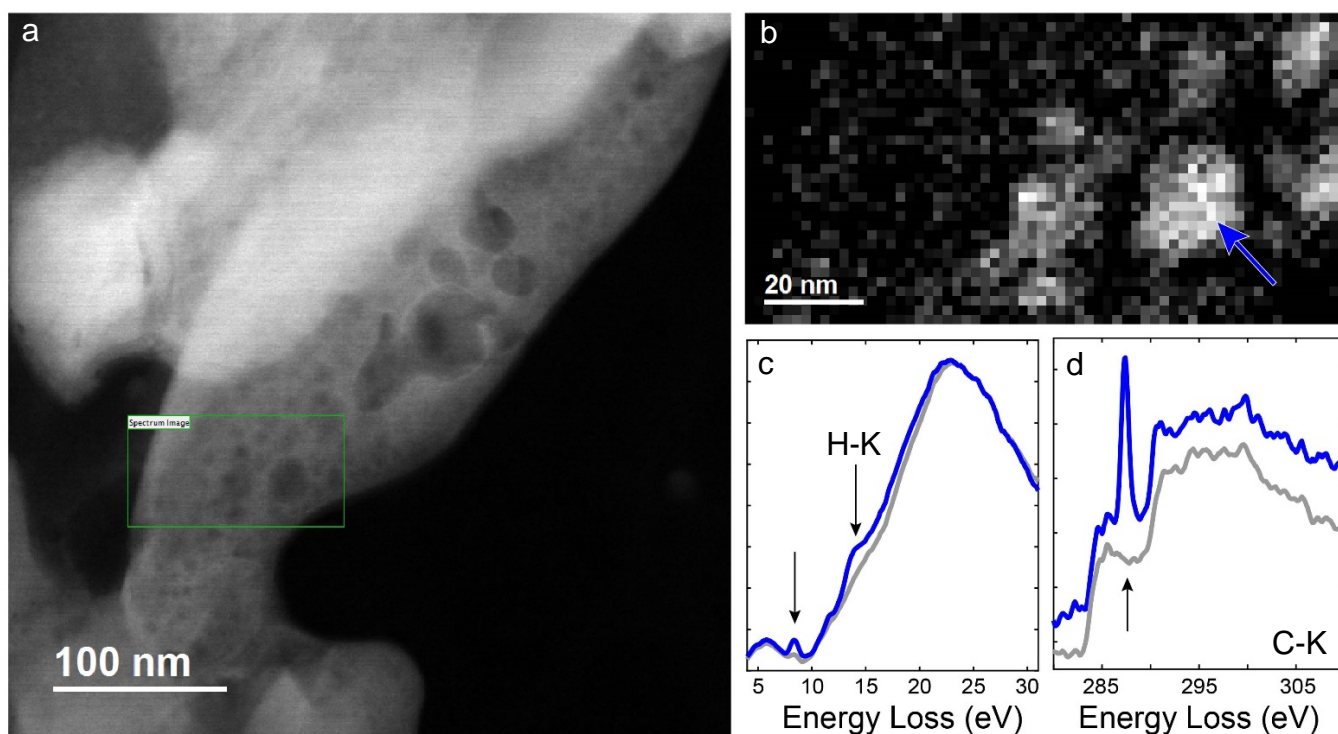


Figure 2. (a) HAADF image of particle in U2012A-3C with a vesicular rim. (b) Window map of 8.5 eV peak from region outlined by green box in (a). (c) Low loss spectra from the bright vesicle highlighted in (b) (blue) and surrounding material (gray) showing peaks at ~ 8.5 eV and ~ 13 eV, indicating the presence of hydrogen in the vesicles. (d) Carbon K-edge spectrum showing a large peak at 287.4 eV spatially associated with H-filled vesicles. The peak is indicative of C-H bonds. Amorphous carbon spectrum from the grid substrate (gray) is shown for comparison.

References

- [1] Bradley, J.P., et al. (2014) *PNAS*, *111*, 1732. [2] Brownlee, D., et al. (1998) *LPSC*, *29*, Abstract #1869. [3] Urquhart, S.G., et al. (1997) *Organometallics*, *16*, 2080. [4] Hitchcock, A.P., and I. Ishii (1987) *Journal of Electron Spectroscopy and Related Phenomena*, *42*, 11. [5] Burgess, K. and R. Stroud (2017) *LPSC*, *48*, Abstract # 1076.

Simulating Space Weathering of a Carbonaceous Chondrite via Pulsed Laser Irradiation

Michelle Thompson¹, L. P. Keller¹, R. Christoffersen², M. J. Loeffler^{3,4}, R. V. Morris¹, T. G. Graff², and Z. Rahman²

¹ARES, NASA JSC, Houston, TX 77058

²Jacobs, NASA Johnson Space Center, Mail Code XI3, Houston, TX, 77058

³NASA GSFC, Greenbelt, MD 20771

⁴Northern Arizona University, Department of Physics and Astronomy, Flagstaff, AZ 86011

Introduction: Grains on the surfaces of airless bodies are continually exposed to irradiation from solar wind ions and micrometeorite impact events. These processes, collectively known as space weathering, alter the microstructure, chemical composition, and spectral properties of surface soils [1-2]. While much work has been done to understand space weathering of lunar and ordinary-chondritic materials e.g., [3-5], the effects of these processes on hydrated carbonaceous chondrites is not yet well-understood. Analysis of the space weathering of carbonaceous materials will be critical for interpreting remote sensing reflectance data and for understanding the nature of samples returned by missions targeting primitive, organic-rich airless bodies, e.g., Hayabusa2 and OSIRIS-REx.

Prior to sample return, we can simulate space weathering processes in the laboratory. Micrometeorite impacts can be simulated through pulsed-laser irradiation, and recent experiments have shown the spectral properties of carbonaceous materials are altered by such simulated weathering events e.g., [6-8]. However, the resulting type of alteration i.e., reddening vs. bluing of the reflectance spectrum, is not consistent across all experiments. Further, the microstructural and crystal chemical effects of many of these experiments have not been well characterized, making it difficult to attribute spectral changes to specific mineralogical or chemical changes in the samples. Here we report results of pulsed laser irradiation experiments on chips of the Murchison CM2 carbonaceous chondrite to simulate micrometeorite impact processing.

Samples and Methods: We performed three separate pulsed laser experiments by scanning a Nd-YAG laser (wavelength of 1064 nm, average energy per pulse of 48 mJ, similar to [9]) (1) once, (2) twice, and (3) five times over the surface of the sample, in order to simulate various degrees of surface exposure. Glass slides were placed above the samples enabling the collection of the recondensed vapor plume produced by the irradiation, similar to [10]. We obtained reflectance spectra (0.3-2.5 μm) from unirradiated and 1x-irradiated samples, as well as of the vapor deposit of the 1x-irradiated sample. We have analyzed the morphological and chemical effects of the 1x-irradiated samples using the JEOL 7600F field emission scanning electron microscope (SEM) with x-ray detector system at JSC. From this sample, we have prepared electron transparent thin sections from the vapor deposit, the meteorite matrix, and several individual mineral phases using the FEI Quanta 3D focused ion beam (FIB) instrument. These sections were analyzed using the JEOL 2500SE scanning transmission electron microscope (STEM) equipped with a Thermo thin window energy-dispersive X-ray (EDX) spectrometer. We expect to make similar spectral measurements and prepare sections for STEM analysis for the 2x and 5x-irradiated sections.

Reflectance Measurements: The 1x-irradiated sample is darker (1-2%) than the unirradiated material (Fig. 1a) and the vapor deposit on the glass slide shows strong reddening through the VIS-NIR wavelengths (Fig. 1b).

Chemical and Structural Analysis: Vapor Deposit: The vapor deposit is microstructurally and chemically complex, composed of several individual layers ranging between 30-350 nm in thickness. The first layer is a uniform (~50 nm) amorphous layer containing embedded nanoparticles. Quantitative EDX maps indicate the composition of this layer is enriched in Fe, and includes S, Si, and O. Overlying this initial deposit in several locations are thicker (up to 250 nm) deposits composed of Mg, Si, Fe, and Ca (in localized regions). There are vesicles and nanoparticles distributed throughout this layer. The outermost layer is thin (30-50 nm) and EDX maps indicate it is enriched in volatile species including Fe and S, and includes embedded nanoparticles. The

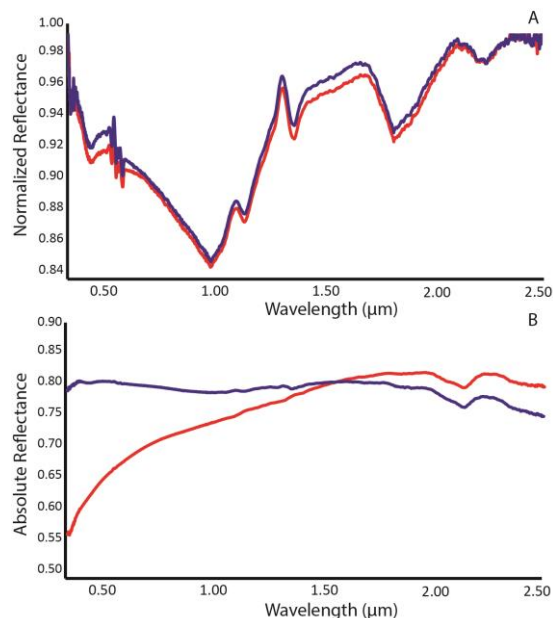


Figure 1: Reflectance spectra of the A) Surface of the irradiated Murchison meteorite (red) compared to the raw sample (blue), and B) The glass slide with the deposit on it (red) compared to the plain glass slide (blue).

nanoparticles distributed throughout the individual layers range in size from 2–30 nm in diameter and selected area electron diffraction (SAED) indicates at least three individual phases are present in the nanoparticle-bearing deposits including troilite (FeS), pentlandite ((FeNi)₉S₈), and magnetite (Fe₃O₄).

Matrix: The SEM images show the irradiated fine-grained matrix material has a distinctive ‘frothy’ texture, exhibiting sub- μm voids uniformly distributed across the surface. TEM analyses of the surface of the irradiated matrix provide evidence of melting including amorphous spherules and droplets. These melt products are up to 500 nm in thickness, are often vesiculated, and contain embedded nanoparticles. Quantitative EDX maps indicate the elemental composition of the melt layers includes Fe, Mg, Si, and S, although volatile species such as Fe and S are depleted in the melt layer relative to the underlying matrix. The matrix phases maintain crystallinity up to the boundary with the melt layer, with only localized regions of amorphization. The nanoparticles range in size from 5-50 nm and EDX maps indicate they are dominated by Fe-Ni-Sulfides.

Olivine: Bright-field STEM images of an olivine grain indicates there is an amorphous melt layer of uniform thickness (~15 nm) on the surface of the grain. EDX maps indicate this layer has an elemental composition that includes Ca, Al, Mg, Si, and Fe, with more refractory species like Ca and Al in higher concentrations than in the underlying grain. Superimposed on this refractory deposit is a thicker, irregular (up to 70 nm) amorphous layer with high concentrations of embedded nanoparticles ranging in size from 2-30 nm.

Fe-Ni-Sulfide: The surface of the Fe-Ni-Sulfide grain exhibits melt textures including droplet-like features. Dark-field STEM and correlated HRTEM images of the melted region indicate localized areas near the surface of have recrystallized. Vesicles are present within 500 nm of the surface and range in size from 5-100 nm. Quantitative EDX maps indicate there is no significant difference in the composition of the sulfide grain at the melted and recrystallized surface when compared to the interior region of the sample (Fig. 2).

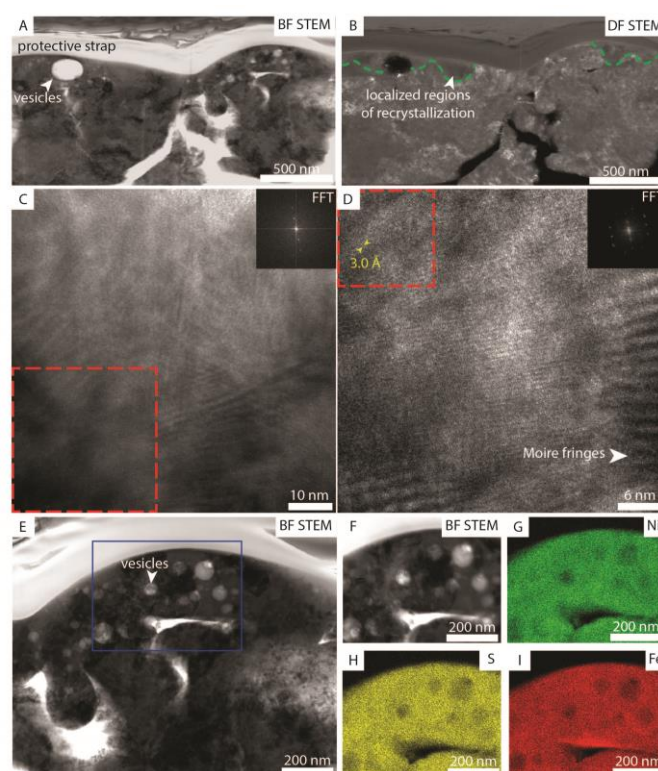


Figure 2: Analysis of the irradiated sulfide grain reveals A) melt features and vesicles in BF STEM, and B) areas of recrystallization in DF STEM, outlined by the dashed green lines. HRTEM images in C) and D) show zones of amorphization and short range order, highlighted by FFTs of regions bounded by the red dashed boxed. Measurements of the lattice fringes indicate spacings are consistent with pentlandite. Round vesicles are shown in E). The region outlined by the blue box in E) is shown in F). The chemical composition of this region is shown by EDX maps of G) Ni, H) S, and I) Fe, indicating the composition is consistent between the irradiated area and the underlying material.

Implications for Space Weathering of Primitive Bodies: The observed elemental fractionation between melt and vapor deposits influences the mineralogy of the nanoparticle population produced during space weathering events. The diversity of nanoparticle phases identified here indicates that the space weathering of carbonaceous materials is more complex than their lunar and ordinary chondrite-style counterparts. In addition, volatile species (including water) may play a significant role in the formation of space weathering features in carbonaceous surface materials. The prevalence of Fe-Ni-Sulfide and presence of Fe-Oxide nanoparticles may contribute to the unpredictable spectral behavior of some experimentally-produced samples. As such, an improved understanding of the optical characteristics of nanophase Fe-Ni-Sulfides is necessary to predict their effect on the spectral properties of airless body surfaces.

References: [1] Hapke B. 2001. *Journal of Geophysical Research-Planets* 106: 10,039-10,073. [2] Pieters C. M. and Noble S. K. 2016. *Journal of Geophysical Research-Planets* 121: 1865-1884. [3] Keller L. P. and McKay D. S. 1997. *Geochimica et Cosmochimica Acta* 61: 2331-2341. [4] Noguchi T. et al. 2014. *Meteoritics and Planetary Science* 49: 188-214. [5] Thompson M. S. et al. 2014. *Earth, Planets, and Space* 66: 1-10. [6] Sasaki S. et al. 2001. *Nature* 410: 555-557. [7] Loeffler M. J. et al. 2008. *Icarus* 196: 285-292. [8] Gillis-Davis J. J. et al. 2017. *Icarus* 286: 1-14. [9] Matsuoka M. et al. 2015. *Icarus* 254: 135-143. [10] Keller L. P. et al. 2013. Abstract 2404, 44th LPSC.

Development on non-destructive muonic X-ray analysis: Application to Earth and Planetary Science

K. TERADA¹, A. SATO¹, K. NINOMIYA¹, Y. KAWASHIMA¹, K. SHIMOMURA^{1,2},
D. Tomono¹, G. YOSHIDA¹, Y. KAWAI¹, T. OSAWA³ and S. TACHIBANA⁴

¹Osaka University, ²High Energy Accelerator Research Organization.
³Japan Atomic Energy Agency and ⁴Hokkaido University

The muon is a lepton with a mass of $105.7 \text{ MeV}/c^2$, approximately 200 times heavier than the electron. So far, electron-induced characteristic X-ray analysis has been widely used to determine chemical compositions of materials in Earth and Planetary Science. In recent years, analysis of characteristic X-rays from muonic atoms, in which a muon is captured, has attracted attention because both a muon beam and a muon-induced characteristic X-ray have high transmission abilities, of which energies are about 200 times higher (e.g., muonic carbon-K α is 75keV, whereas electron-induced carbon-K α is 0.3 keV). It is known that muonic X-ray analysis has great advantages in several ways; (1) non-destructive elemental analysis from light to heavy elements, (2) depth profile analysis, (3) isotopic measurement for heavy elements and (4) investigation of chemical condition (redox-state). Such a non-destructive muonic X-ray analysis has a great potential to characterize precious extraterrestrial samples returned by spacecrafts such as Hayabusa2 and OSIRIS-REx in 2020's.

Following our successful detection of muonic X-ray spectra from carbonaceous chondrites, Murchison and Allende with intense pulsed Muon beam at J-PARC [1], we have developed on muonic X-ray analysis at the MuSIC (MuSIC; MUon Science Innovative Channel at Osaka University, [2, 3]), and obtained the fundamental data for quantitative analysis of planetary materials [4]. Using one of the world-leading intense direct current muon beam source, we successfully detected characteristic muonic X-rays of Mg, Si, Fe, O, S and C from Jbilet Winselwan CM chondrite, of which carbon content is about 2 wt%, and the obtained elemental abundance pattern was consistent with that of CM chondrites. We also checked Muon irradiation damage of pellets of mixed organic chemical reagents (alanine, glucose, paraformaldehyde, phenanthrene, and stearic acid) after 3–12 hour exposure to check the irradiation damage, and confirmed that they do not show any systematic changes with either the exposure time or the depth, and are not different from those of non-exposed samples within the variation of initial reagent mixtures. We also performed the muonic X-ray analysis of terrestrial PbS (Galena) for Pb isotopes measurement and iron meteorite to check the feasibility of chemical condition (redox-state) measurement. At the symposium, we will report on our recent progress of muonic X-ray analysis and discuss on a future prospect for applications for earth and planetary science.

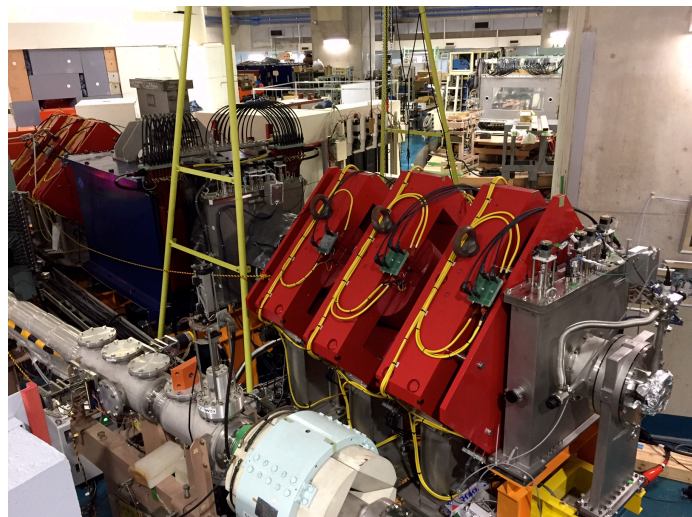


Figure 1: Direct-current Muon beam line at MuSIC, Osaka University.

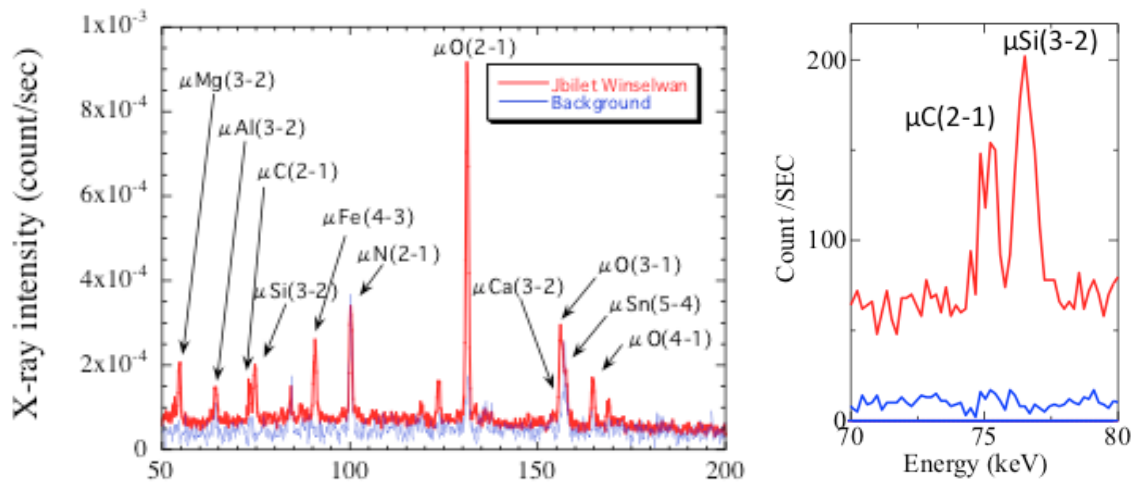


Figure 2: Muonic X-ray spectra of Jbilet Winselwan CM2 chondrite.

References

- [1] Terada, K. *et al.* 2014. *Sci. Rep.* **4**, 5072; DOI:10.1038/srep05072 [2] Hino, Y. *et al.* 2014. *Nuclear Physics B (Proc. Suppl.)* **253-255**, 206-207. [3] Cook, S. *et al.* 2017. *Physical Review Accelerators and Beams* **20**, 030101.

Using X-ray Microfocus Spectroscopy to determine Cometary and Asteroidal Parent-Body Processes

L. J. Hicks¹, J. C. Bridges¹, T. Noguchi², M. C. Price³, J. E. Wickham-Eade³,
M. J. Burchell³, J. L. MacArthur¹, G. M. Hansford¹, A. L. Butterworth⁴

¹Leicester Institute for Space and Earth Observation, Space Research Centre, University of Leicester, UK. (ljh47@le.ac.uk)

²Faculty of Arts and Science, Kyushu University, Japan. ³School of Physical Sciences, University of Kent, UK.

⁴Space Sciences Laboratory, University of California at Berkeley, USA.

Since the *Stardust* and *Hayabusa* missions, we have investigated a selection of these returned cometary and asteroidal samples using Beamline I-18 at the *Diamond Light Source* synchrotron in UK, measuring Fe-K X-ray Absorption Spectroscopy (XAS) and transmission X-ray Diffraction (XRD). Such techniques are essential to determine the origin and evolution of fine grained planetary materials, and in particular we have identified evidence for water-rock reaction on the Wild2 parent body.

I-18 X-ray microfocus spectroscopy

Beamline I-18 has an energy range 2.0-20.7 keV and a spot size reduced to $\sim 2.5 \mu\text{m}$. X-ray Fluorescence (XRF) can provide chemical compositions, with XRF maps providing the opportunity to accurately locate features of interest at the micron-scale. Fe-K XAS measurements typically range 6900-7500 eV at variable energy resolutions 1.0-10 eV, with higher resolution steps of 0.1 eV focused over the XAS near-edge (XANES) region 7090-7150 eV necessary to accurately determine minor shifts and variations in the $1s \rightarrow 3d$ transition pre-edge peak structure and absorption edge. The $1s \rightarrow 3d$ centroid position is estimated from the intensity-weighted average energy position over the pre-edge peaks, and the absorption edge position is the energy at which intensity is 0.5 of the normalized spectra. Comparisons are made to reference materials, in particular the ferric content of silicates are estimated by comparing pre-edge centroids with the ferrous-ferric energy shift in standards [1]. Combined with XRF mapping, producing XANES maps can reveal any variations in the ferric content. Additionally, in-situ measurements of transmission-XRD are acquired at 13 keV, with observable 2θ ranging 5.5° - 38.4° , corresponding to d -spacings 9-1.5 Å.

Identifying magnetite in Comet Wild 2 samples

Initial investigations of Comet Wild 2 samples returned by *Stardust* identified mostly high temperature ferromagnesian silicates [2], but additional constituents have included CAI's and chondrule-like fragments, suggesting links between carbonaceous chondrites and the Wild 2 material [3].

Hicks et al. (2017) [4] investigated the terminal grains of eight *Stardust* aerogel tracks, which include terminal grains identified as near pure magnetite Fe_3O_4 . *Stardust* track C2045,4,178,0,0 (#178) featured a magnetite terminal grain measuring $10 \mu\text{m}$ in diameter, and a $5 \mu\text{m}$ magnetite terminal grain in track C2065,4,187,0,0 (#187), both visibly identified via XAS structure (Figure 1). In particular, absorption edge positions at 7121.5 and 7121.0 eV, and $1s \rightarrow 3d$ centroid positions estimated at 7113.1 and 7113.5 eV, closely resemble that of a magnetite powder standard with edge and centroid positions at 7120.8 eV and 7113.2 eV respectively. A small positive shift of up to ~ 0.5 eV in the Wild 2 grains, compared to the magnetite standard, could be due to a minor Ni^{2+} content identified with XRF, which replaces some Fe^{2+} , resulting in a higher $\text{Fe}^{3+}/\Sigma\text{Fe}$ content, thus a positive shift in the energy of the Fe-K XAS spectra.

In-situ transmission XRD analyses also identified magnetite with 2θ peaks at d -spacings 1.48 Å, 1.61 Å, 1.71 Å, 2.10 Å, 2.42 Å, 2.53 Å, and 2.96 Å for the cometary #178 (Tg1a and Tg2) and #187 (Tg1), closely matching the 2θ peaks a magnetite reference material. However, with unit cell dimensions ranging 8.355-8.370 Å for the cometary grains being slightly lower than that of a pure magnetite at 8.387 Å, this shift also suggests a Ni-bearing magnetite. Raman analyses performed at University of Kent also confirmed a Ni-bearing magnetite. Material in other *Stardust* tracks, identified via XAS analyses on I-18 at *Diamond*, include olivine (#177, #178, #187), pyroxene (#189, #190), Fe,Ni-metal (#170, #176), and Fe,Ni-sulfide (#187, #188) [4].

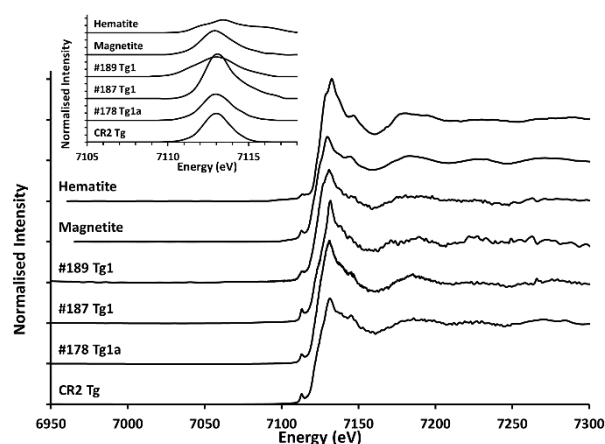


Figure 1. The Fe-K XAS and pre-edge centroid (inset) of terminal grains in tracks #178 (Tg1a), #187 (Tg1), and #189 (Tg1), and an analogue CR2 terminal grain (Tg) shot into aerogel, compared to powdered magnetite and hematite standard reference material.

Magnetite grains are prominent in carbonaceous chondrites, if they have been oxidised and aqueously altered [5], thus the presence of magnetite in the Wild 2 mineral assemblage suggests further affinities to carbonaceous chondrites, probably resulting from hydrothermal alteration of the co-existing FeNi and ferromagnesian silicates in the cometary parent-body. Exploring this hypothesis further, powdered NWA 10256 CR2 chondrite material was shot into aerogel at 6.1 kms⁻¹, using a light gas gun [6], simulating the conditions of the *Stardust* collection. Fe-K XAS identified CR2 magnetite terminal grains (Figure 1) establishing the likelihood of preserving magnetite during capture in silica aerogel.

Itokawa ferromagnesian silicates and LL5 chondrite

Initial analyses of the Itokawa asteroid particles returned by *Hayabusa* had already found mineralogical, petrological, and oxygen isotopic affinities to LL5-6 chondrites [7,8,9]. We used Fe-K XAS to investigate the relative abundance of Fe³⁺ and Fe²⁺ ions in the ferromagnesian silicates of the Itokawa grains, comparing them to the Tuxtuac LL5 chondrite meteorite.

Noguchi et al. (2014) [10] investigated four samples from the first *Hayabusa* touch-down location: RB-QD04-0008; RB-QD04-0011; RB-QD04-0015; and RBQD04-0024. These samples, each embedded in epoxy resin, featured olivine with trace amounts of opaque minerals (0011 and 0015), olivine and high-Ca pyroxene (0008), and low-Ca pyroxene with plagioclase and small (<2 µm) opaque minerals (0024).

Fe-K XAS for the olivines (Figure 2) estimated absorption edges and 1s→3d centroids at 7119.5-7119.8 eV and 7112.5-7112.6 eV respectively, indistinguishable from those estimated for the Tuxtuac olivine and in terrestrial olivine. Edges and centroids for the low-Ca Itokawa pyroxene (7119.7 eV and 7112.6 eV), and the high-Ca Itokawa pyroxene (7119.4 eV and 7112.6 eV), are also indistinguishable from Tuxtuac and from Fe²⁺ in terrestrial augite. EXAFS analyses of the high-Ca Itokawa pyroxene suggested a disordered structure which may be partial equilibration or shock. A Ni-bearing phase associated with that high-Ca Itokawa pyroxene (0008) was also measured for Ni-K XAS, finding similarities to taenite in the LL5 Tuxtuac.

The Fe-K XAS analyses suggested a negligible abundance of Fe³⁺ ions in Itokawa and the LL5 ferromagnesian silicates, consistent with the initial analyses [7,8,9]. However, the EPMA analyses of the four Itokawa grains, that followed the Fe-K XAS analysis, suggested a wide range of thermal metamorphism corresponding to petrologic chondrite types LL4 to LL6.

Future XAS investigations of Planetary Sample Returns

As we continue to investigate planetary materials further, and as missions such as *Hayabusa 2* and *OSIRIS-REx* return samples to Earth, more advanced techniques will be essential to analyse micron-sized material, furthering our understanding of planetary formation. Offering similar techniques to I-18, but with higher spatial resolution down to ~50 nm, the new I-14 hard X-ray nanoprobe beamline at *Diamond* offers nanoscale microscopy with an energy range 5-23 keV, capable of XAS, XANES mapping, and XRD. Additionally, the I-08 Scanning X-ray Microscope (SXM) beamline performs XRF and XANES, but in the soft X-ray energy range 0.25-4.4 keV, including Si-K XANES, with a spatial resolution down to ~200 nm.

References

- [1] Berry, A.J. et al., XANES calibration for the oxidation state of iron in silicate glass. *Am. Mineral.*, 88, 967-977, 2003.
- [2] Zolensky, M. et al., Mineralogy and petrology of Comet 81P/Wild 2 nucleus samples. *Science*, 314, 1735-1739, 2006.
- [3] Westphal, A.J. et al., The future of Stardust science. *Meteorit. Planet. Sci.*, in press, 2017.
- [4] Hicks, L.J. et al., Magnetite in Comet Wild 2: Evidence for parent body aqueous alteration, *Meteorit. Planet. Sci.*, in press, 2017.
- [5] Hutchison, R., *Meteorites: A petrologic, chemical and isotopic synthesis*. Cambridge Press, 2004.
- [6] Burchell, M.J., et al., Hypervelocity impact studies using the 2 MV Van de graff accelerator and two-stage light-gas gun of the University of Kent at Canterbury. *Meas. Sci. Technol.*, 10, 41-50, 1999.
- [7] Nakamura T. et al., Itokawa Dust Particles: A Direct Link Between S-Type Asteroids and Ordinary Chondrites. *Science*, 333, 1113-1116, 2011.
- [8] Yurimoto H. et al., Oxygen Isotopic Compositions of Asteroidal Materials Returned from Itokawa by the Hayabusa Mission. *Science*, 333, 1116-1119 2011.
- [9] Nakamura E. et al., Space environment of an asteroid preserved on micrograms returned by the Hayabusa spacecraft. *Proc. Nat. Acad. Sci.*, 109, 4031-4032, 2012.
- [10] Noguchi, T. et al., Mineralogy of four Itokawa particles collected from the first touchdown site, *Earth Planets Space*, 66: 124, 2014.

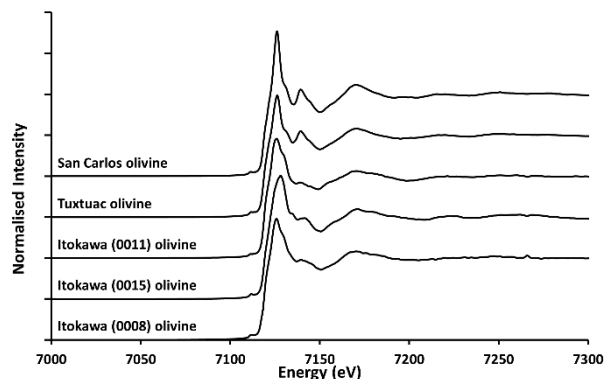


Figure 2. The Fe-K XAS for olivine in three Itokawa particles, the Tuxtuac LL5 chondrite, and a terrestrial olivine (San Carlos).

The Astromaterials X-Ray Computed Tomography Laboratory at Johnson Space Center

Ryan A. Zeigler, Poorna Srinivasan, Lindsay P. Keller, Francis McCubbin, and Daniel M. Coleff

Astromaterials Research and Exploration Division, NASA JSC, Mailcode XI, 2101 NASA Parkway, Houston, TX 77058

Overview: The Astromaterials Acquisition and Curation Office at NASA's Johnson Space Center (hereafter JSC curation) is the past, present, and future home of all of NASA's astromaterials sample collections. JSC curation currently houses all or part of nine different sample collections. Our primary goals are to maintain the long-term integrity of the samples and ensure that the samples are distributed for scientific study in a fair, timely, and responsible manner, thus maximizing the return on each sample. Part of the curation process is planning for the future, thus we also perform fundamental research in advanced curation initiatives. Advanced Curation is tasked with developing procedures, technology, and data sets necessary for curating new types of sample collections, or getting new results from existing sample collections [1]. As part of these advanced curation efforts we are augmenting our analytical facilities. A micro X-ray computed tomography (micro-XCT) laboratory dedicated to the study of astromaterials came online within the JSC Curation office this summer, and we plan to add additional facilities that will enable non-destructive (or minimally-destructive) analyses of astromaterials in the near future (micro-XRF, confocal imaging Raman Spectroscopy). These facilities will be available to: (1) develop sample handling and storage techniques for future sample return missions, (2) be utilized by PET for future sample return missions, (3) be used for retroactive PET-style analyses of our existing collections, and (4) for periodic assessments of the existing sample collections. Here we describe the new micro-XCT system, as well as some of the ongoing or anticipated applications of the instrument.

Instrument: We have installed a Nikon XTH 320 micro-XCT system in JSC curation. It has four interchangeable X-ray sources: 180 kV nano focus transmission source, 225 kV reflection source with multi-metal target (Mo, W, Ag, Cu), a 225 kV rotating target (W) reflection source, and a 320 kV reflection source. The system also has a 16-bit, 400 mm² (2000 x 2000 pixel) CCD detector, as well as a heavy-duty stage that will accommodate large (up to 30 cm) and heavy (up to 100 kg) samples. The multiple sources, high-resolution detector, and large stage allow us the flexibility to analyze a wide range of sample sizes. The 180 kV transmission source will allow for high resolution (submicron) scans on small samples (less than ~5 mm), whereas the 225 kV and 320 kV sources will allow scans of larger samples at resolutions on the order of 10s or 100s of microns per voxel depending on the sample size. The maximum size high-density rock sample that can be scanned has yet to be determined, but test scans on basalt samples >15 cm in diameter have been successful.

Discussion: High-intensity XCT scanners have been used to study astromaterials (and other geologic samples) for over 15 years [2-3], and the practice is becoming ever more prevalent. They have a wide range of scientific uses, including (but certainly not limited to) measuring porosity, determining the modal abundance and 3D distribution of phases inside samples, and identification of fabrics or strain patterns in samples. In addition to their use for research, XCT scans have increasingly been utilized as a part of the astromaterials curation process, beginning with meteorites [4-5], and more recently with the Apollo samples [6]. Their utility in

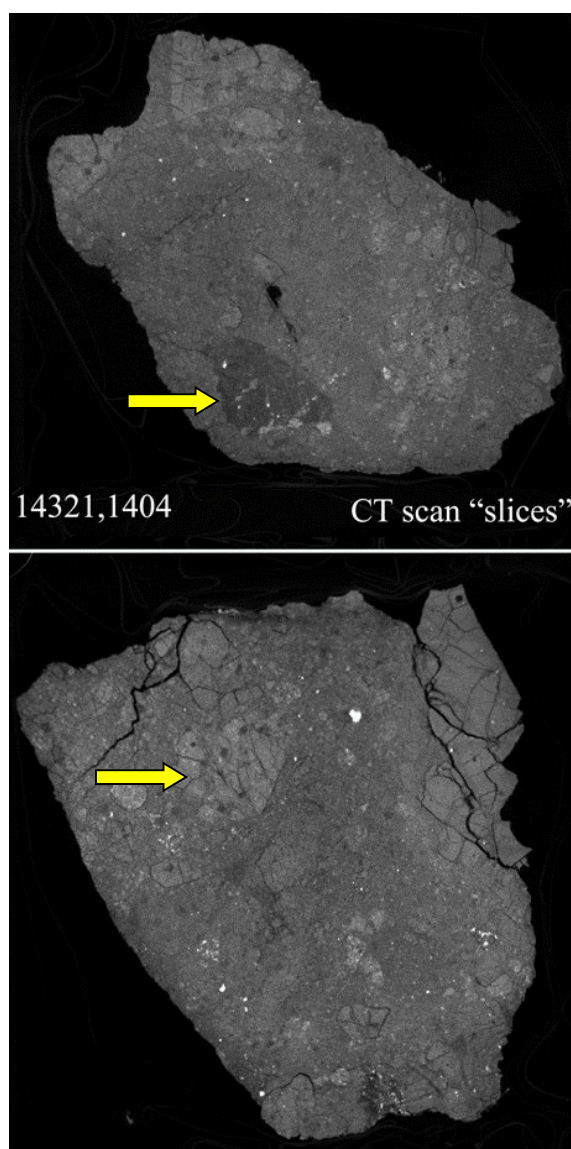


Figure 1: Slices of the micro-CT scan of sample 14321,1404. Brightness of the phases are proportional to x-ray attenuation (a measure of composition and density of the phase). Yellow arrows highlight interesting feldspathic (top) and mafic (bottom) clasts. Sample is ~ 6 cm in diameter.

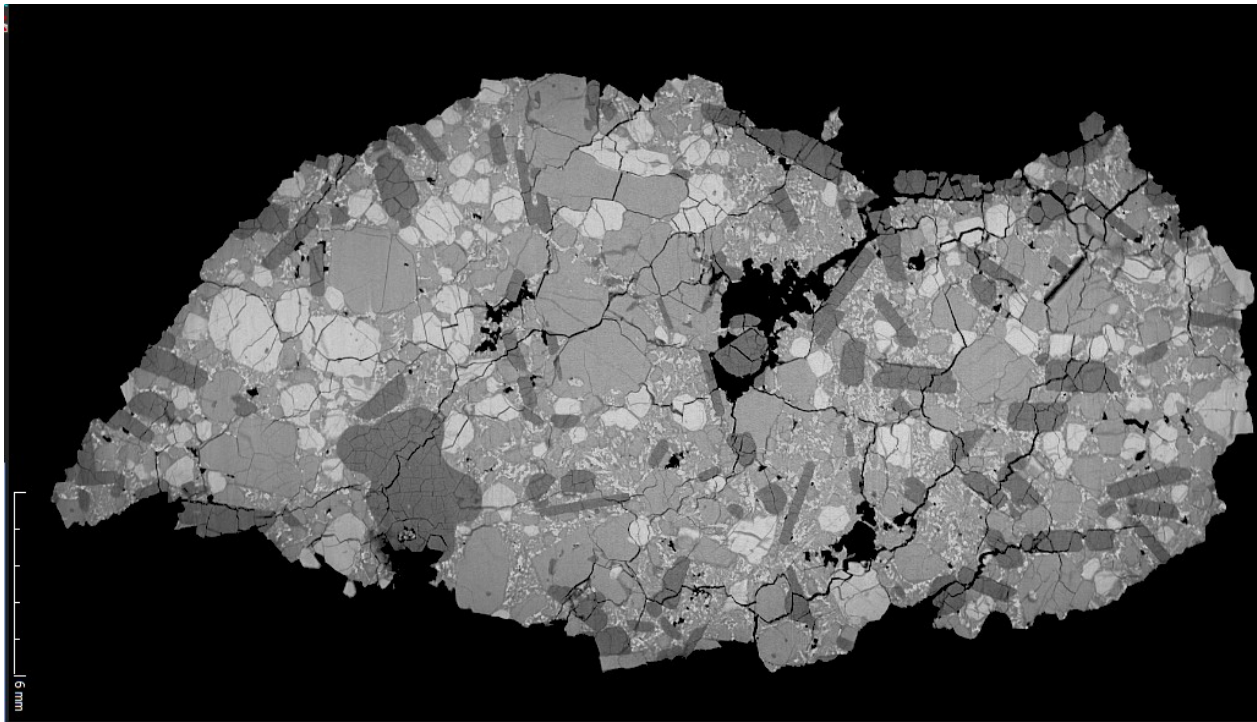


Figure 2: Single 2D slice of the micro-CT scan of ungrouped achondrite NWA 11119 showing the igneous textures and major mineralogical phases within the sample. Sample is ~ 3 cm long.

curations lies in their ability to non-destructively map out the phases and voids within a sample. As an example, we have scanned several large Apollo polymict breccias, and we were able to identify and tentatively classify the lithologies in these clasts. The samples can then be subdivided, either through sawing or careful chipping, and those “new” clasts made available to scientists. In addition to the myriad curatorial uses, we have begun to use the XCT system as an integral part of coordinated analyses of astromaterials. Two examples of this are the mapping of textures within ungrouped achondrite NWA 11119 (Figure 2), as well as a newly acquired unclassified carbonaceous chondrite from Morocco (Figure 3). In each case, the XCT scans were able to characterize the major phases with the meteorites, and identify areas of interest for additional higher resolution study (e.g., by TEM). The penetrative nature of the XCT scans allows for astromaterials samples to be analyzed within sealed low-density containers, preserving the pristinity of the samples. The XCT technique is not completely non-destructive, however. A recent study by [7] has shown that XCT scans of meteorites can alter the natural radiation dose of the sample. The number of techniques where this is applicable (e.g., thermo-luminescence) is limited, however. Nevertheless, XCT scans could cause damage for other types of studies (e.g., organics), and we plan to undertake extensive studies to fully characterize the impact XCT scans have on the samples. In the meantime, the percentage of any one sample that is studied by XCT will be limited to ensure that no irreparable damage is done to an entire sample.

References [1] McCubbin et al. (2017) This Symposium, [2] McCoy et al. (2002) EPSL 246, 102-108. [3] Zolensky et al. (2014) MAPS 49, 1997-2016. [4] Almeida et al. (2014), MAPS 77 abstract #5033. [5] Smith C. L. (2013) MAPS 76, abstract #5323. [6] Zeigler (2014) 45th LPSC, abstract #2665. [7] Sears, et al. (2016) MAPS 51.4, 833-838.

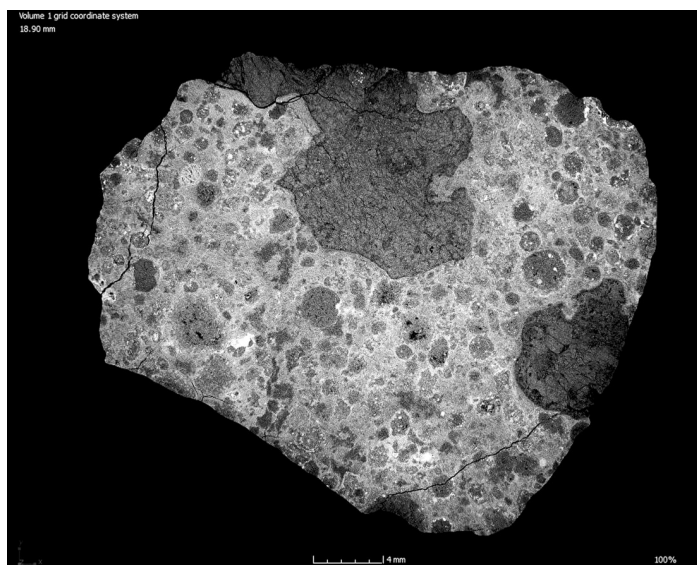


Figure 3: Single slice of the micro-CT scan of an unclassified Moroccan carbonaceous chondrite. Large dark grey areas are large zoned CAIs. Sample is ~4 cm in diameter.

Reproduction of GEMS-like materials in the induction thermal plasma system

Tae-Hee Kim¹, Akira Tsuchiyama¹, Junya Matsuno¹, Aki Takigawa^{1,2}

¹Mineralogical Laboratory, Division of Earth and Planetary Sciences, Kyoto University, Kyoto, Japan

²The Hakubi Center for Advanced Research, Kyoto University, Kyoto, Japan

Amorphous silicates are considered to be one of the most primitive materials of the solar system and some of them came from pre-solar environments. Chondritic porous interplanetary dust particles (CP IDPs) contain abundant amorphous silicate grains of ~100 nm in size with Fe-Ni and FeS nanoparticles known as GEMS (glass with embedded metal and sulfides) [1,2]. Solar and interstellar origins of GEMS have been proposed [1, 2]. Experimental study on non-equilibrium condensation of GEMS-like materials is crucial for determination of the GEMS origin.

The ITP system (induction thermal plasma) offers rapid vaporization condition by a discharged high temperature flame (~10,000 K) and rapid cooling rate ($10^4\sim 10^5$ K/s). Amorphous silicates with metallic iron nanoparticles inside, which are similar to the characteristics of GEMS, were experimentally reproduced using an ITP system [3]. In order to constrain the formation condition of GEMS, we systematically changed ITP operation conditions and performed evaporation and condensation experiments with a new ITP system [4].

The ITP system used in the present study was JEOL TP-40020NPS with 6 kW RF plasma torch. We carried out the vaporization and condensation experiments with a mixed Ar-He plasma flame in the system of Si-Mg-Fe-Na-Al-Ca-Ni-O with the averaged chemical composition of GEMS [1] without sulfur. The plasma generating condition was controlled by selection of a plasma forming gas injecting direction (tangential and radial flame patterns) and reactor pressure (30 and 70 kPa). The tangential flame of the thermal plasma provides more higher cooling rate than the radial flame, and higher reactor pressure enhances the vaporization degree of the starting material [4].

All run products show presence of amorphous silicate, metallic iron, and FeNi in X-ray diffraction spectra and peaks of amorphous silicate at ~10 μm in the FTIR spectra. TEM observation shows that the run products have a variety of textures; amorphous silicate grains from <a few nm to >100 nm with or without aggregation and with or without embedded metallic iron or iron nickel nanoparticles. Among them, the most similar nanomaterial with GEMS was reproduced in a tangential flame condition at 70 kPa (Fig. 1). Although the condensation condition was not quantitatively investigated yet, the present result shows that GEMS-like nanomaterial can form in a limited parameter range of the ITP system, which indicates that the formation conditions and environments of actual GEMS might also be limited.

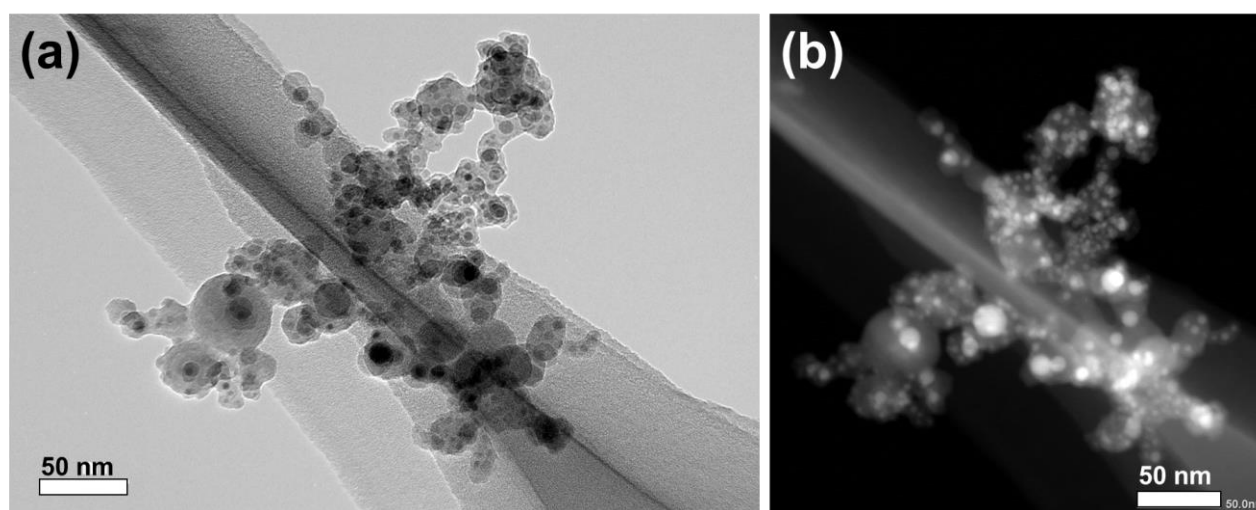


Figure 1. (a) TEM image and (b) STEM-HAADF image of metal embedded amorphous silicate grains produced in tangential plasma flame condition at 70 kPa.

References

- [1] Keller L. P. et al. 2011. *Geochimica et Cosmochimica Acta*, 75:5336
- [2] Bradley J. P. et al. 2004. *Astrophysical Journal*, 17:650
- [3] Matsuno J. 2015. Ph.D. thesis, Kyoto University.
- [4] Kim T. H. et al. 2017. Proceeding #P2-33-7. ISPC 23 (International Symposium on Plasma Chemistry)